FACULDADE DE ENGENHARIA DA UNIVERSIDADE DO PORTO

# Relative acoustic localization with USBL (Ultra-Short Baseline)

**Paula Alexandra Agra Graça**

WORKING VERSION


Master in Electrical and Computers Engineering

Supervisor: José Carlos Alves

Co-supervisor: Bruno Ferreira

September 16, 2020

# Resumo

Dispositivos robóticos programáveis como *Autonomous Underwater Vehicles* (AUVs) são excelentes meios para exploração subaquática, já que são capazes de executar missões de longa duração com variadas possibilidades de aplicação e objetivos. Neste sentido, o conceito de mula AUV surgiu como mecanismo útil que periodicamente recolhe dados dos AUVs em missão. Para que tal seja possível, é necessário implementar um sistema de localização e posicionamento robusto que permite aos AUVs encontrarem outros veículos de forma a aproximarem-se deles eficientemente.

A presente dissertação foca-se na implementação de mecanismos que levam a um aumento de precisão na localização subaquática usando um sistema USBL (Ultra-Short Baseline), para curtas e longas distância. Primeiro, é descrito o design da arquitetura de um modulo capaz de melhorar a precisão da medida dos tempos de chegada de sinais enviados por uma fonte acústica. De seguida, é conduzido um estudo sobre possíveis métodos de avaliação do desempenho de uma configuração de sensores, já que consiste num aspecto crucial na precisão de estimação. Por último, o método de seleção adaptativa de configurações é apresentado, o qual serve como ferramenta que seleciona um conjunto de hidrophones, a partir de um grupo discreto em posições fixas, que leva a uma maior precisão na localização. Este método pretende retificar problemas que surgem em sistemas USBL clássicos.

Após a implementação, todos os mecanismos desenvolvidos foram sujeitos a testes detalhados em simulação que validam o seu funcionamento e demonstram resultados satisfatórios em condições controladas. Adicionalmente, foram realizados testes no tanque do DEEC e em mar aberto para avaliar as melhorias alcançadas nas medidas dos tempos de chegada.

# Abstract

Robotic programmable devices such as Autonomous Underwater Vehicles (AUVs) are great means for underwater exploration, as they are capable of executing long term missions with many possible applications and goals. In this regard, the concept of mule AUVs arises as a valuable mechanism to periodically collect data from survey AUVs during the missions. In order to achieve this, a robust localization system needs to be implemented allowing the mule AUV to find the other vehicle and draw near it efficiently.

The present dissertation focuses on the implementation of mechanisms that lead to an increase in underwater localization precision using an USBL (Ultra-Short Baseline) system, for both short and long range. Firstly, it is described the architecture design of a module that is capable of improving the precision of the time of arrival measurement of signals sent by an acoustic transmitter. Then, a study is conducted on possible methods for evaluating a sensor configuration performance, as it consists on a crucial aspect in estimation precision. Lastly, the adaptive configuration selection method is presented, which serves as a tool that selects a set of hydrophones, from a discrete group in fixed positions, that leads to the highest localization precision. This method intends to rectify issues that arise from classic USBL systems.

After implementation, all developed mechanism were subjected to comprehensive simulated tests that validate its function and demonstrate successful results with controlled conditions. Additionally, tests were performed in DEEC's tank and in open sea to evaluate the achieved improvement on the time of arrival measurements.

*"A curiosidade leva por um lado a escutar às portas*
*e por outro a descobrir a América"*

Eça de Queirós

# Contents

# List of Figures

# List of Tables

# Abbreviations

| | |
|---|---|
| ADC | Analog to Digital Converter |
| AUV | Autonomous Underwater Vehicle |
| BPSK | Binary Phase Shift Keying |
| CC | Cross-Correlation |
| CORDIC | COordinate Rotation DIgital Computer |
| DEEC | Departamento de Engenharia Electrotécnica e de Computadores |
| FIM | Fisher Information Matrix |
| FIR | Finite Impulse Response |
| FPGA | Field-Programmable Gate Array |
| FSK | Frequency-Shift Keying |
| GCC | Generalized Cross-Correlation |
| HDL | Hardware Description Language |
| LBL | Long Baseline |
| LOS | Line-of-sight |
| LUT | Lookup Table |
| MF | Medium Frequency |
| ML | Maximum Likelihood |
| RMS | Root Mean Square |
| ROM | Read-Only Memory |
| RSSI | Received Signal Strength Indicator |
| SBL | Short Baseline |
| SNR | Signal-Noise Ratio |
| TDE | Time Delay Estimation |
| TDoA | Time Difference of Arrival |
| ToA | Time of Arrival |
| ToF | Time of Flight |
| USBL | Ultra-Short Baseline |

# Chapter 1

# Introduction

This chapter intends to specify the context of the present dissertation, describing the considered scenario, technologies and conditions in which the proposed solution is useful. Based on this, the two main goals of the present research work are established. Lastly, it is explained how the document is structured, including a concise summary of each chapter's content.

## 1.1 Context and Motivation

Today, the deep blue ocean still represents a relevant topic of research in the scientific community as it constantly rises new unexplained mysteries. Up to now, only 15% of the entire ocean floor is mapped based on collected data [1]. As such, it seems essential to create efficient research tools to improve the discovery of information.

Robotic autonomous underwater vehicles (AUVs) are great means for diverse applications in underwater exploration using variable resource requirements and duration, such as monitoring structures installed in shallow waters or exploring the deep ocean floor for scientific purposes. Particularly in long-term missions, the AUV usually navigates underwater, resorting to docking systems to allow extended navigation periods, until the end of the mission when it returns to the base station. Thus far, the data that is being collected is typically not accessible by any processing system.

A method that is used to resolve this limitation is employing additional mule AUVs, whose goal is to travel near the survey AUV, collect its data during the mission's term and return in a relatively short time period. This allows the data to be periodically processed during the mission, which facilitates the definition of future courses for the mission, such as shortening its duration or sending additional commands. In the mentioned localization system, high precision is key as it allows the AUVs to reach very short distances between them when they approach each other. This typically influences the achievable debit of data transfer in common communication solutions, which is a key aspect in data muling.

The described process can only be achieved if the mule AUV is able to locate the other vehicle and draw near it. For such application, USBL (Ultra-Short Baseline) systems prove to

have several advantages comparatively to other localization methods, such as optical, radio and inertial based techniques. The main advantages are the achievable range, limited error and lower sensibility to environment conditions, such as salinity or turbidity. For that reason, in this scenario, a USBL system is used to receive the transmitted signals and calculate the angle of arrival of the acoustic signal, thus the direction that the mule AUV should navigate. Additionally, using a synchronization mechanism, the mule is also able to determine the distance to the acoustic source and thus the vehicles' relative positions.

In such scenario, the USBL system needs to meet specific requirements to assure a reliable localization. Since the acoustic source can be located anywhere, it is essential that the estimation is accurate for both short and long range distances. Additionally, the system needs to have line of sight in any direction, which is compromised from the start by deploying the sensors on an AUV. Typically, the available USBL commercial solutions do not tackle these issues simultaneously, so the development of such system constitutes a technological challenge.

Therefore, this dissertation intends to develop a method that improves relative localization of AUVs using reconfigurable USBL systems. All the contemplated tools and complementary mechanisms are carefully explained throughout the document.

This research work falls under the scope of activities developed by the Center of Robotics and Autonomous Systems of INESC TEC. It is integrated in the GROW project which focuses on exploring the use of AUVs as data mules for long duration missions.

## 1.2 Objectives

The goal of the present work is to study and propose an adaptive configuration selection method, which assumes the integration of several hydrophones in a USBL system to allow selecting the set of sensors that minimizes the estimation error. This aims to achieve high estimate accuracy for both short and long range distances and continuously provide a set of hydrophones that have line of sight with the target, which can be located anywhere. In order to attain this, a comparative study is developed on tools that allow to compare the performance of sensors configurations in order to select the most reliable option. Then, the proposed system is presented in detail and validated with comprehensive simulations.

Building upon previous developments on the USBL system, it is also intended to achieve a more rigorous calculation of the TDoA to enable a more precise localization. By associating this improved calculation with the correlation measurement already implemented, it is expected to obtain a more precise ToA measurement.

## 1.3 Document Structure

The present document is partitioned into six chapters, which are summarized in this section.

Chapter 2 offers an overview on background concepts about underwater acoustics, localization estimation and positioning systems, followed by USBL available commercial

solutions and developed technology for a similar purpose. Then it focuses on angle of arrival determination methods and optimization mechanisms that are typically employed.

After reviewing the literature, chapter 3 intends to clarify the problem that is being resolved in this thesis. The research hypothesis is stated as well as the research questions that are discussed and intended to be further explored. The chapter ends with the clarification of the used validation methods for the work.

Chapter 4 presents and explains the developed hardware design for the phase difference calculation. Then, three different approaches are presented for systematic comparison between the performance of a sensor configuration. These are supported with simulation experiments which allow to draw conclusions on the preferred approach.

Chapter 5 details the developed dynamically reconfigurable configuration method. The theoretical specifics and thought process are laid out and the mechanism is then validated through simulations.

Lastly, chapter 6 gives the final remarks about the developed work and mentions research work which could be further developed in the future.

# Chapter 2

# State of the Art

This chapter presents the fundamental concepts of underwater acoustics engineering for localization and positioning of aquatic autonomous vehicles.

## 2.1 Underwater acoustic channel

Although satellite based navigation systems are the most commonly used for positioning and localization at the earth surface, the used radio signals are highly absorbed by the water and thus inappropriate for underwater localization and communications. Therefore, the state of the art solutions for long range localization and communications in the underwater environment rely on the propagation of acoustic signals.

The natural limitations of acoustic channels combined with the properties of an underwater environment, result in challenges and limitations in developing communication and localization systems [2]:

- Long propagation delays make it unmanageable for underwater acoustic networks to employ some common data networks' mechanisms, such as acknowledgment-based protocols;
- Variable speed of the acoustic signals due to variations in temperature and density;
- Limited bandwidth, as the attenuation of acoustic waves increases with frequency;
- The path of acoustic signals is not a straight line since the sound waves are bent due to sound speed variation along the water column and reflected or blocked in many different surfaces and objects, which may lead to the incorrect detection of the line-of-sight (LOS) signal;
- Attenuation and asymmetric signal-to-noise ratio, which arises from SNR depending on depth and frequency with complex behaviors that depend on the characteristics of the environment;

Underwater localization systems based on acoustic signals are the only effective way to work in distance ranges up to a few kilometers, as opposed to optical or radio-frequency based systems.

However, these always unreliable characteristics lead to a significant degree of uncertainty as, in practice it is impossible to know the exact speed and path of a sound wave along the path it actually travels.

This section presents hereinafter a more detailed overview on various concepts that affect the underwater communication channels, such as the sound speed, multipath phenomena, the Doppler effect, signal attenuation and signal-to-noise ratio.

### 2.1.1 Speed of sound

The oceanic environment has a complex sound propagation model, as it comprises many variants.

Acoustic signals' propagation speed is mainly related to two factors: compressibility and density. The water density can be characterized by the temperature, salinity and pressure,which is associated with depth [3]. Figure 2.1 exhibits a generic sound speed profile in relation to depth. The water surface is commonly a mixed layer that results in an approximately constant sound speed. After this layer, it suffers a significant decrease, usually reaching the lower tangible speed, which results from the variation of temperature that characterizes the thermocline layer. From that point forward, pressure is the greatest influencer on speed of sound, so it increases relatively proportionally to depth.

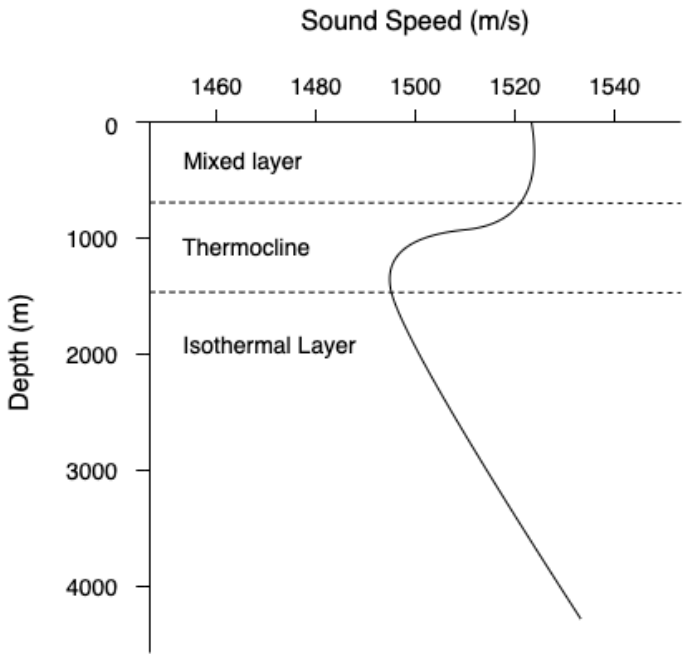


Figure 2.1: Generic sound speed profile

The empirical equation 2.1 [3] is a simplified translation of the behavior of the sound speed $c$ in meters per second, with relation to the temperature $T$ in $^{o}$C, the salinity $S$ in parts per thousand

and the depth $z$ in meters.

$$c = 1449.2 + 4.6T - 0.055T^2 + 0.00029T^3 + (1.34 - 0.01T)(S - 35) + 0.016z \quad (2.1)$$

The varying sound speed throughout the water column causes the signals not to propagate in a straight line from a transmitter to a receiver. Therefore, the ToA calculation would not be precise in positioning system such, as USBL.

### 2.1.2 Multipath

Multipath occurs when signals suffer distortion that originate multiple propagation paths, leading to a change in their original characteristics. This phenomenon is originated by diverse factors that cause distortion in the underwater channels, typically affecting the water composition, such as water temperature and depth. The signal distortions caused by multipath include signal fading, which is usually modeled by Rayleigh fading channel theory [4], varying operation frequency, time-variant propagation delays, among others.

The multipath behavior can be distinguished depending on depth, in shallow water paths and deep water paths since they demonstrate distinct propagation effects:

**Shallow water paths** In shallow water, the acoustic signals can be reflected or refracted on the surface, where attenuation is generally weaker then at the bottom of the ocean. There it suffers a higher attenuation depending on the soil material, frequency and incidence angle. Figure 2.2 represent a typical multipath caused by reflection on the sea surface and bottom.

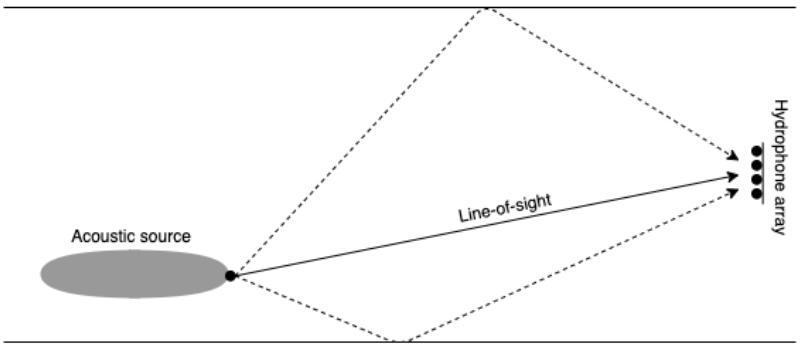


Figure 2.2: Illustrative example of shallow water multipath

**Deep water paths** In deep water, there are essentially six types of propagation paths, detailed bellow, whose channel model equations can be consulted in [4]. These rely on the notion that signals are bent towards the characteristics that lead to a slower propagation speed, such as a temperature and depth decrease.

- *Surface reflection*: the signal is reflected on the sea surface, where the attenuation depends on its acoustic roughness.

- *Surface duct*: the signal gets confined in a surface layer, where the sound velocity increases with depth, due to varied thermal conditions in deeper layers, which causes it to bend the wave path to the surface and bounce back when reaching the subsequent layer.
- *Bottom bounce*: the signal is reflected on the bottom of the ocean, suffering attenuation dependent on the soil material.
- *Convergence zone*: it depends on the sound speed profile and water depth that characterizes the channel. When the temperature decreases the signal has a tendency to bent downwards, however when an increase in pressure is reached the signal tends to bent upwards again, originating convergence locations.
- *Deep sound channel*: it is originated in levels that are surrounded by layers with characteristics highly dependent on depth. So, the signal is constantly bent according to the depth that leads to a minimum speed.
- *Reliable acoustic path*: this path occurs when the transmitter is positioned in very deep water and the receiver is near the surface. Although the signal is bent downwards due to decreased temperature, when it reaches a certain depth it is bent upwards making the communication channel reliable.

The multipath phenomena is a very common factor that affects underwater communication mechanisms such as the USBL systems. For such case, the ray bending that occurs between the transmitter and the receiver can cause the signal to assume different paths and affect the resulting estimations. For instance, if the signal deviates from the direct path, then the angle of arrival would not be accurate and the ToA increases leading to an increased error on the range estimation.

### 2.1.3 Doppler Effect

In a communication and localization system between two entities moving with non-zero relative velocity, if a transmitter sends a signal with a certain operation frequency to the receiver, then the perceived frequency by the receiver will suffer a shift from the original signal. This frequency difference is expressed as a Doppler shift and explained by the Doppler Effect.

The magnitude of the generated frequency shift can be expressed as a ratio 2.2, where the transmitter-receiver velocity is compared to $c$, the speed of sound [5].

$$a = \frac{v}{c} \tag{2.2}$$

Autonomous Underwater Vehicles (AUVs) usually move with velocities in the order of few meters per second. Therefore, the $a$ factor mentioned above has a significant value and needs to be considered when implementing synchronization systems, as well as developing estimation algorithms.

dúvida - relatively low sound speed propagation ??

In certain localization and communication systems, it is critical to correct the Doppler effect because data can be compromised (e.g. FSK modulated signals, in which information is codified into frequency changes). A simple Doppler compensation process was proposed in [6], with the intent of integrating it in a system that detects phase-modulated binary sequences using cross-correlation.

This phenomenon can also be explored to determine the relative velocity between two devices, by measuring the frequency deviation with respect to the frequency expected to be received.

The Doppler effect can influence the USBL system's performance since the computation of TDoAs depend on the perceived phase difference between the arriving signals, which are directly related to the operation frequency. Therefore, a frequency shift would make the positioning system have a distorted perception of the phase differences and thus the signal's angle of arrival.

### 2.1.4 Attenuation and signal-to-noise ratio

When considering underwater communication systems, it is essential to quantify the attenuation of the channel, i.e. the part of the signal's energy that is absorbed by the surroundings. In underwater channels, this absorbance is frequency variable and also depends on physical characteristics of the water, as salinity and temperature.

The underwater acoustic channel has a particular model that describes its attenuation path loss $A(d, f)$, given in logarithmic scale by equation 2.3 [7].

$$10\ log(A(d,f)) = 10\ k\ log(d) + d \times 10\ log(a(f)) \tag{2.3}$$

From the equation, $d$ is the distance from the transmitter to the receiver in kilometers (Km), $f$ is the operating frequency in kilohertz (KHz), $10klog(d)$ represents the spreading loss that describes how the sound level (in decibel, dB) decreases as the sound wave spreads, $d \times 10\ log(a(f))$ is the absorption loss that a signal suffers during its propagation path, $k$ is the spreading factor that is related with the considered configuration (e.g. cylindrical, spherical, etc.), $a(f)$ is the absorption coefficient that can be obtained through the equation in [7].

Noise is another factor that is considered when analyzing a real underwater acoustic channel, as it defines the signal-to-noise ratio (SNR) that characterizes the channel. The SNR depends on the attenuation level, which increases with frequency, and the noise, which decays with frequency. Consequently, the SNR varies over the signal bandwidth and it is asymmetric. The equation 2.4 [5] expresses this relationship, where $S_d(f)$ represents the power spectral density of the transmitted signal.

$$SNR(d,f) = \frac{S_d(f)}{(A(d,f))\ N(f)} \tag{2.4}$$

Signals that are heavily attenuated can become an issue when dealing with acoustic positioning systems, such as USBL systems. If the transmitted signals suffer high attenuation

then it can be unfeasible to rigorously detect the signal in the receiver, therefore compute the range or angle of arrival of the transmitter. Additionally, in case of having a noisy environment it can be difficult to identify the intended acoustic signal, since it can be blended with the noise and not be distinguishable.

## 2.2 Range estimation for underwater localization

Underwater localization takes into consideration the distance between the target object to track and the reference point. As consequence, it is always relevant to apply methods that effectively determine this range.

There are two main types of techniques that are used to achieve such objective: the Received Signal Strength Indicator (RSSI) and the Time Delay Estimation (TDE).

### 2.2.1 Received Signal Strength Indicator

The Received Signal Strength Indicator (RSSI) method is based on the strength of the signal that reaches the target. It determines the distance between the target and the reference node by analyzing the received signal strength and comparing it with an underwater attenuation model that is range dependent [3].

Since the underwater acoustic channel suffers from multipath, time variance and high overall path loss, the RSSI technique is typically not adequate for long range underwater applications. However, in short range communications such effects can be sufficiently attenuated for this technique to be used.

### 2.2.2 Time Delay Estimation

Time Delay Estimation (TDE) mechanisms imply a pair of nodes, the transmitter and the receiver, to measure the range between them. This distance is based on the time that it takes for a signal to travel from the reference point to the target. The accuracy of these techniques depends mainly on the environment conditions, which include the water properties and the surrounding reflection surfaces that cause multipath. Therefore, the mechanisms are susceptible of variable errors according to the location and characteristics of its employment.

There are three main categories that divide TDE methods, which are Time Difference of Arrival (TDoA), Time of Arrival (ToA) and Time of Flight (ToF).

#### 2.2.2.1 Time of Arrival

Time of Arrival (ToA) is interpreted as the time delay between the transmission of a signal in the reference node until its reception on the target node. Although this is the conceptually simplest method to employ, it requires synchronization between the nodes since the target entity needs to know the instant when the signal was sent to be able to calculate the difference.

Considering a generic transmitted signal *s(t)*, the received signal can be expressed as (2.5), where $\tau$ represents the time of arrival and *n(t)* is white noise with zero mean [8].

$$r(t) = s(t-\tau) + n(t) \tag{2.5}$$

#### 2.2.2.2 Time of Flight

Time of Flight (ToF) measures essentially the round-trip travel time between two nodes. The transmitter node sends a query signal to the receiver node, which has an integrated transponder that responds transmitting a signal back within a know time delay. The ToF is then estimated as the time interval from the moment the first signal is transmitted until the moment the second signal is received by the same node.

This method may be used without additional synchronization systems as it assumes that the response signal is sent after the received one and the intrinsic transmitting delays are known.

#### 2.2.2.3 Time Difference of Arrival

The Time Difference of Arrival (TDoA) is a technique that compares the time of arrival of a signal to different hydrophones in order to estimate the angle of arrival of the acoustic signal. The array of reception hydrophones have known relative positions among them so that is is possible to compare the different times of arrival or phase differences. This method can be employed using a uni-directional signal or a round trip communication.

There are several algorithms and mathematical models that can be employed to execute the TDoA method, such as Cross-Correlation and Maximum Likelihood.

- **Cross-Correlation**

  The Cross-Correlation (CC) method is used to represent the strength relationship between two signals.

  Considering two distanced hydrophones in the same environment and an acoustic signal *s(t)*, $x_1(t)$ and $x_2(t)$ are the signals received by each of the two hydrophones. Equations (2.6) and (2.7) [9] express the mentioned signals in relation to $w_1(t)$ and $w_2(t)$ that are Gaussian noise coefficients uncorrelated with the source, the delay $\tau$ and an attenuation function $\alpha$.

$$x1(t) = s(t) + w1(t) \tag{2.6}$$

$$x2(t) = \alpha s(t-\tau) + w2(t) \tag{2.7}$$

  Then the cross-correlation function can be expressed as (2.8). However, since the observation time is finite then function $R_{x_1x_2}$ can only be estimated, originating equation (2.9).

$$R_{x_1x_2}(\tau) = E[x_1(t)\ x_2(t-\tau)] \tag{2.8}$$

$$\widehat{R}_{x_1x_2}(\tau) = \frac{1}{T-\tau}\int_{\tau}^{T} x_1(t)x_2(t-\tau)dt \tag{2.9}$$

The Cross-Correlation technique uses a prefilter $\psi(f)$ equal to 1, being the simplest method of its kind.

The cross-correlation method is one of the traditional methods for measuring the time delay between two hydrophones by using the similarity between signals from the hydrophones.

- **Generalized Cross-Correlation**

  The Generalized Cross-Correlation (GCC) method

  From these expressions,

  From these expressions, the generalized cross-correlation function between signals $x_1(t)$ and $x_2(t)$ is given by (2.10). The function $G_{x_1x_2}(f)$ is the spectrum of the cross-correlation. Function $\psi(f)$ represents a prefilter and it is essentially the distinctive parameter that originates different methods of cross-correlation, since it should depend on different environments and properties, as SNR.

$$R_{x_1x_2}(\tau) = \int_{-\infty}^{\infty} \psi(f)G_{x_1x_2}(f)\ e^{i2\pi f\tau}df \tag{2.10}$$

$$T = argmax\ _{t\in R^+} Rx_1x_2(\tau) \tag{2.11}$$

The variable $T$, expressed in (2.11), represents the maximum correlation value that indicates the time delay $\tau$ between two signals, which is the main outcome of Time Delay Estimation.

- **Maximum Likelihood**

  The Maximum Likelihood (ML) method is a variation of Cross-Correlation which uses the prefilter $\psi(f)$ represented mathematically by 2.12, where $\gamma_{12}(f)$ is a function of spectrum of cross-correlation $G_{x1x2}(f)$ and spectrum of auto-correlations $G_{x1x1}(f)$, $G_{x2x2}(f)$ as expressed in 2.13 [9].

$$\psi(f) = \frac{|\gamma_{12}(f)|^2}{|G_{x1x2}(f)|[1-|\gamma_{12}(f)|^2]} \tag{2.12}$$

$$|\gamma_{12}(f)|^2 = \frac{|G_{x1x2}(f)|^2}{G_{x1x11}(f).G_{x1x11}(f)} \tag{2.13}$$

There is also a version of ML that uses the power spectral densities of the signals, which can be helpful for calculations in various applications.

## 2.3 Localization estimation

In networks with multiple nodes is typical to use localization estimation to establish position relationships between elements. The operation principal is usually to have a set of reference nodes with known positions so that it is possible to determine the relative positions between each reference node and the target.

An extensive comparison of different localization schemes for underwater sensors networks can be consulted in [10].

### 2.3.1 Triangulation

Triangulation is a method of localization based on the measurement of angles which are related to the reference beacons and the target object.

#### 2.3.1.1 Three-Object Triangulation

The simplest method of this category is the Three-Object Triangulation, which considers a configuration as illustrated in figure 2.3. It is assumed that the location of the beacons is pre-configured and the environment is obstacle-free. $\lambda_{12}$ is the angle formed by the intersection of the straight lines [O,1] and [O,2]. Similarly, $\lambda_{31}$ is the angle formed by the intersection of the straight lines [O,1] and [O,3]. Using these two sets of nodes, we can trace circumferences that include their coordinates and as a consequence their intersection will correspond to the location of the target.

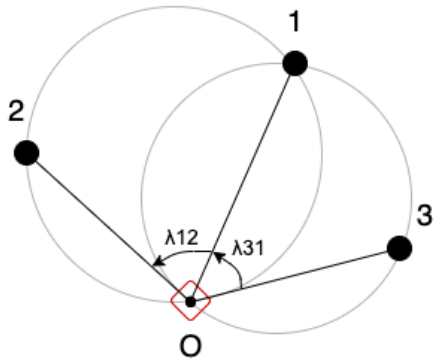


Figure 2.3: Three-Object Triangulation

Although this is a very straightforward technique to implement, it does not cover all possible scenarios, namely when the three beacons and the object are all placed in the same circumference or when the environment has obstacles between nodes.

#### 2.3.1.2 Geometric Triangulation algorithm

A more complex method relies on the Geometric Triangulation algorithm.

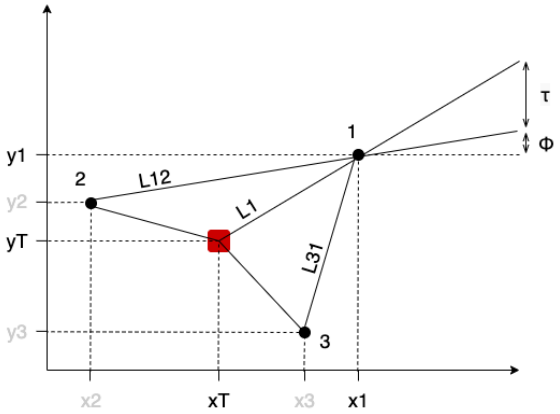


Figure 2.4: Geometric Triangulation algorithm

Considering a Cartesian plane with defined lengths L1, L12 and L31, as shown in image 2.4, it is possible to establish trigonometrical relationships that estimate the location of the object within the created triangular areas. The position of the target is given by coordinates (xT,yT) and can be calculated through equations 2.14 and 2.15. (x1,y1) represents the location of beacon 1 and L1 is the distance between this beacon and the object. The trigonometric relationships for calculating the mentioned variables can be consulted in [11].

$$xT = x1 - L1 * cos(\phi + \tau) \tag{2.14}$$

$$yT = y1 - L1 * sin(\phi + \tau) \tag{2.15}$$

### 2.3.2 Trilateration

Trilateration is a technique that does not rely on calculations using angles but instead it uses distances to locate an object.

Considering a scenario with three reference beacons, the distance between the target and each one of the beacons is taken as the radius of a circumference. By doing this, it is possible to obtain three circumferences that intersect each other. With only two circumferences, there are two possible locations for the object, however, when added the third circumference the exact location is obtained. The 2D coordinates are obtained by solving systems of equations with the circle equation 2.16 [12], where $(x_i, y_i)$ is the beacon coordinates and $r_i$ is the distance between the beacon and the object.

$$(x - x_i)^2 + (y - y_i)^2 = r_i^2 \tag{2.16}$$

Trilateration is commonly used in underwater acoustic localization, as it used to find a relative position of the target in two dimensions and additionally determines the depth as third dimension, by using a pressure sensor with high accuracy.

### 2.3.3 Multilateration

Multilateration is a generalization of the trilateration technique, as it uses the same conceptual principal with multiple reference beacons instead of exactly three. In this method, the employment of *n+1* nodes will allow to determine *n* coordinates [13]. For example, determining the position (x,y,z) of a target, would require to resolve a system of equations using 2.17. $(x_i, y_i, z_i)$ is the coordinates of the beacon and $d_i$ is the distance between the beacon and the target.

$$(x-x_i)^2 + (y-y_i)^2 + (z-z_i)^2 = d_i^2 \tag{2.17}$$

Distributed mechanisms, such as multilateration, are usually divided in three phases of positioning [10]:

- Distance estimation between the reference nodes and target object, usually using TDoA or ToF mechanisms;
- Position estimation, usually obtained by solving a system of linear equations through mathematical efficient techniques;
- Final refinement of the measurement in order to improve accuracy.

As an alternative to solve localization issues using circumferences, multilateration can also take advantage of a hyperbola-based localization method. Considering a target at (x,y) and three reference beacon with coordinates $(x_i, y_i)$, $(x_j, y_j)$ and $(x_k, y_k)$, we have that the difference between times of arrival $t_i$ and $t_j$ to nodes $i$ and $j$, respectively, can be related to the distance between nodes, as expressed in 2.18 [13]. $d_i$ and $d_j$ are the distance from node $i$ and $j$, respectively, to the target object.

$$d_i - d_j = c * (t_i - t_j) = \sqrt{(x-xi)^2 + y - yi)^2} - \sqrt{(x-xk)^2 + y - yk)^2} \tag{2.18}$$

## 2.4 Positioning Systems

Positioning systems are used to track the underwater position of a vehicle or other object, in relation to reference structures of transponders called *baseline stations*. These systems are classified based on the distance between the baseline stations. The configurations that will be explained are Long Baseline (LBL), Short Baseline (SBL), Ultra-Short Baseline (USBL) and the inverted versions of all above.

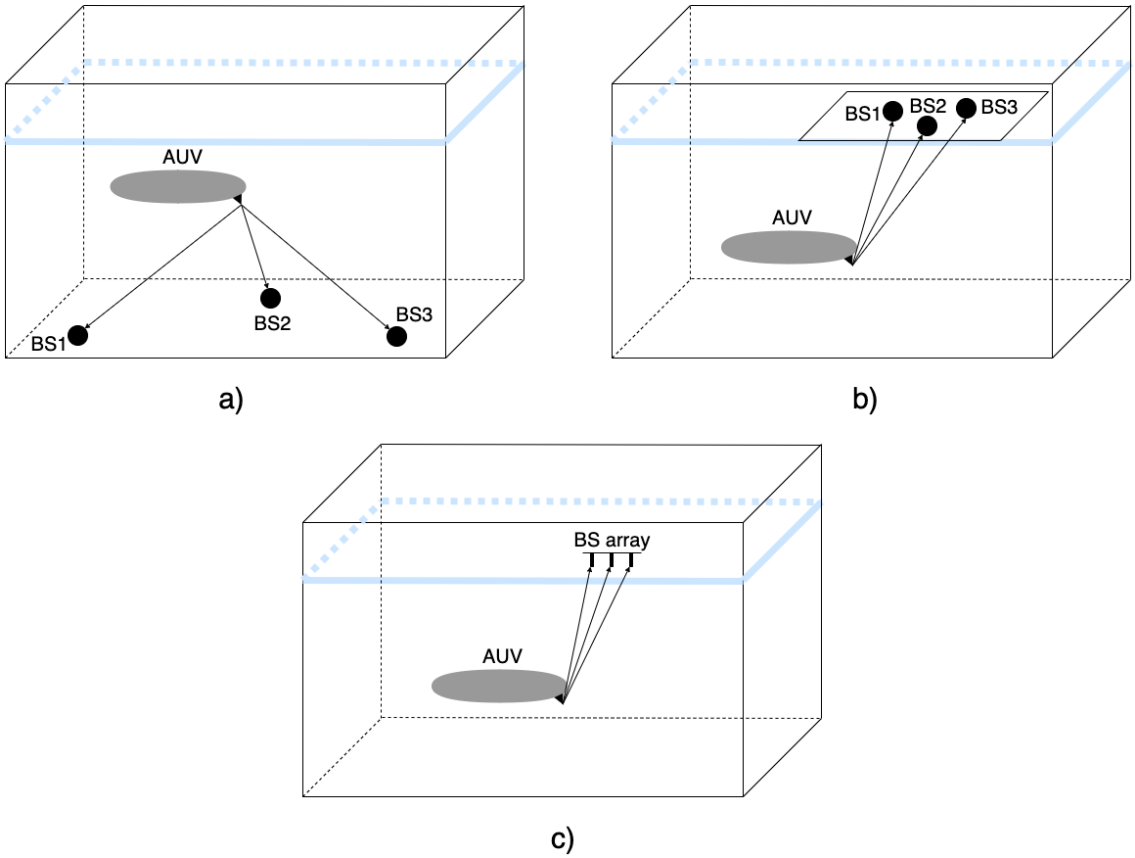


Figure 2.5: Generic configuration of: a) LBL; b) SBL; c) USBL

### 2.4.1 Long Baseline (LBL)

Long Baseline systems use a positioning method with large distances between baseline stations, with range typically from 50m to more than 2000m and usually similar to the distance between object and transponders [9]. A typical LBL configuration is represented in figure a) 2.5.

The LBL method uses at least three transponder stations deployed usually on the sea floor, allowing to execute trilateration. Additionally, a transducer is integrated on the object to be tracked.

A complete localization procedure starts with the vehicle sending an acoustic signal which is received by the transponders. Thereafter the transponders transmit a response and, by analyzing the Time of Flight of the communication, the system can determine the distance between the vehicle and each base station. Then the relative position of the vehicle is determined through trilateration. Additionally, if the transponders have known geographic positions, it is possible to infer the vehicle geographic position.

As this technique presents large distances between the object and the base stations, the typical 1m to few centimeters accuracy is considered to be high because it will not compromise the localization of the vehicle.

### 2.4.2 Short Baseline (SBL)

Short Baseline systems are characterized by having distances around 20m to 50m between baseline stations [2] and use an operation procedure similar to the LBL method. However, the transponders are usually placed in a moving platform, which assures a fixed relative position between them. A typical SBL configuration is represented in figure b) 2.5.

The position of the vehicle to be tracked can be determined by translating the Time of Flight between the multiple transponders and the object into a distance value, which is achieved by equation 2.19 [14]. The $t_i$ corresponds to the propagation time of the signal from the vehicle to the $i$th transponder, $c$ is the speed of sound, [$x_{b_i}$, $y_{b_i}$ and $z_{b_i}$] is the coordinate position of the transponder.

$$\sqrt{(x_{b_i}-x)^2+(y_{b_i}-y)^2+(z_{b_i}-z)^2} = c * t_i \tag{2.19}$$

In a SBL system, when the distance between baseline stations is increased the accuracy improves and, contrarily, when the mentioned distance decreases the accuracy deteriorates, which can raise some deployment challenges.

### 2.4.3 Ultra-Short Baseline (USBL)

Ultra-short baseline systems are composed essentially by one baseline station, with an array consisting of several traducers distanced typically less than the wavelength [15], and a transponder

integrated on the object to be tracked. It is usually used in underwater positioning in shallow areas of the sea, as represented in figure c) 2.5.

Similarly to the previously mentioned procedures, the USBL positioning method relies on the Time of Flight of the exchanged signals. However, the traducers are too spatially close from each other to execute an accurate trilateration. Instead, it is measured the phase difference or time-delay difference of the received signal between every traducer, in order to estimate the azimuth and distance to the acoustic source.

Assuming a three dimensional scenario for the positioning system, as represented in figure 2.6, the object's coordinates are given by equations 2.21, 2.22 and 2.23 [16]. The $\lambda$ corresponds to the wavelength of the of the transmitted signal which depends on its operation frequency, $f$, and it is affected by the speed of sound $c$, as represented equation 2.20. The $d$ represents the distance between hydrophones, $\psi_{12}$ and $\psi_{22}$ are the phase difference between H2 and the other two hydrophones, $H$ is the height of the target object, $X$ is the distance of the target along the x-axis direction, $Y$ is the distance of the target along the y-axis direction and $l$ is the slant distance of the target to the hydrophone.

$$c = f * \lambda \tag{2.20}$$

$$l^2 = X^2 + Y^2 + H^2 \tag{2.21}$$

$$\psi_{12} = \frac{2\pi}{\lambda}[\sqrt{l^2} - \sqrt{(d-X)^2 + d^2 + H^2}] \tag{2.22}$$

$$\psi_{22} = \frac{2\pi}{\lambda}[\sqrt{l^2} - \sqrt{X^2 + (d-Y)^2 + H^2}] \tag{2.23}$$

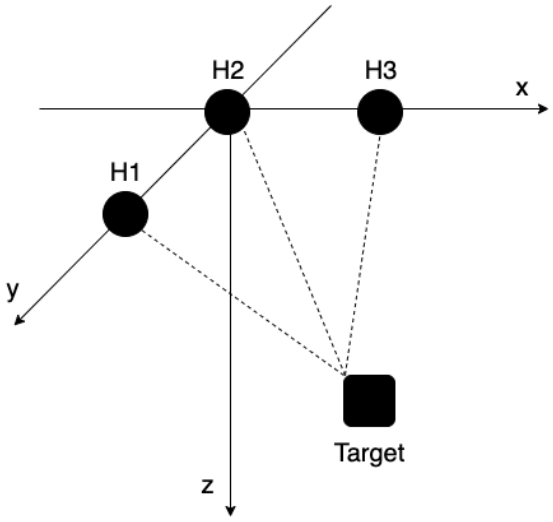


Figure 2.6: USBL system configuration

This is a broadly used technique due to its convenient set up, which allows to have predefined measurements in the order of tens of centimeters and does not require AUV navigation area for the deployment. However it presents the lowest accuracy, comparatively with LBL and SBL, since an

error of few centimeters can be realistically corresponding to an inaccuracy of several meters in the position of the object to be tracked.

### 2.4.4 Inverted Systems

All the previously mentioned positioning techniques use a configuration in which the vehicle to be tracked has a single transducer and there is an external set of transponder to determine the positioning of the said object. However, there is the possibility to benefit from the inverse configuration in some applications. Therefore, there are also the iLBL, iSBL and iUSBL methods, which have the same operation principals as LBL, SBL and USBL, respectively.

## 2.5 Commercial Solutions

There are several commercial solutions for underwater positioning using the ultra-short baseline method. In this section, it will be presented some of the available devices in the market, indicating their main properties and capabilities. Table 2.1 summarizes the systems with most relevance to the present work. The Medium Frequency (MF) bandwidth is attributed to devices whose manufacturer did not specified the actual frequency range.

*Evologics* produces the S2C R USBL series of acoustic modems [17], with Sweep Spread Carrier (S2C) technology [18] which uses a broad frequency range to propagate over large distances with reduced noise. The devices have a fixed 0.01m slant range accuracy and a 0.1 degree bearing resolution. These are essentially divided into two groups:

- High speed mid-range devices: contains the 18/34 transceivers family [19], which presents various options for the USBL antenna beam pattern and it is optimal for transmission in horizontal channels.

- Depth rated long-range devices: includes the 12/24 transceiver [20], which have a directional (70 degrees) USBL antenna and it is optimal for transmission in vertical channels.

*Sonardyne* markets the Ranger 2 systems. The Micro-Ranger 2 [21] is very easy to use without previous experience and it is appropriate for shallow waters, achieving accuracy of 0.2%. The Mini-Ranger 2 is ideal for nearshore missions and it is used for simultaneous tracking of various mobile targets, whose position is updated every 3 seconds.

*Applied Acoustics* offers the Easytrak USBL Systems, which includes the processing software for estimating the position. The Alpha Portable 2655 consists in a very compact structure that includes an array transducer and is capable of reaching a 10cm slant range resolution and a 2 degree RMS.

*Kongsberg* produces the HiPAP family of transducers [22], which can use the Cymbal acoustic protocol (PSK) or the frequency shift (FSK) modulation technique. Particularly the HiPAP 352 is the model with higher number of active transducers and is able to reaches 0.02m of range accuracy.

| Company | System | Bandwidth(kHz) | Connection(kbps) | Range(m) |
|---|---|---|---|---|
| Evologics | S2C R 18/34D USBL | 18-34 | up to 13.9 | 3500 |
| | S2C R 12/24 USBL | 12-24 | up to 9.2 | 6000 |
| Sonardyne | Micro-Ranger 2 | MF | 0.2-9 | 995 |
| | Mini-Ranger 2 | MF | 0.2-9 | 995 |
| Applied Acoustics | Easytrak Alpha Portable 2655 | MF | n.d. | 500 |
| Kongsberg | HiPAP 352 | 21-31 | n.d. | 5000 |

Table 2.1: Overview of commercial solutions

## 2.6 Angle of arrival determination

methods for calculating signal's angle of arrival

## 2.7 Optimization of sensor configurations

When dealing with a localization system which integrates a multiple sensor configuration, it is essential to understand how can the sensor layout be designed so that the estimation is optimized. This section is dedicated to explore some commonly employed methodologies which evaluate the performance of sensor layouts considering determined parameters.

### 2.7.1 Crámer-Rao lower bound

The Crámer-Rao bound is a tool which analyzes the variance of a sensor configuration and determines the minimum bound it can achieve independently from the used estimator. This method assumes the usage of an efficient estimator, which is an optimal estimator for the chosen parameter, and an unbiased estimator, i.e. the real value of the parameter is equal to the expected value.

In this thesis, it is conducted a study based on the Crámer-Rao lower bound, which is generally used to generate a *so-called uncertainty ellipse* [23] that represents the spatial variance distribution of the estimated position. The overall desired result is to find the minimum variance that is related to the chosen configuration geometry, which indicates that it is the optimal solution for estimating a certain position. This method utilizes the Fisher Information matrix (FIM), which measures the quantity of information that can be extracted from an observation vector about a certain parameter.

In order to avoid loss of generality, it is considered a set of N sensors and a settled position for the acoustic source, defined by $s = [x_s, y_s, z_s]^T$. In addition, the position of each sensor is defined as $r_i = [x_{r_i}, y_{r_i}, z_{r_i}]$ and, consequently, the measurement of distance between each sensor and the source is defined as $\mathrm{d}_i = ||s - r_i||$.

Thereafter, the observations vector will be formulated containing the observed times-of-arrival (ToA) of the signal from the acoustic source to each one of the hydrophones, considering their

geometric position. These times contain a noise vector component, which can be approximated to to a Gaussian distribution $n_i \sim \mathcal{N}(\mu, \sigma^2)$. The samples can be calculated through the expression 2.24, where it is considered an initial time of arrival $t_0$. Additionally, c represents the sound speed underwater.

$$t_i = t_0 + \frac{||d_i||}{c} + n_i \tag{2.24}$$

After having the observations matrix, it is established the condition to formulate the Fisher Information matrix, $I(d)$ , which results into equation 2.25.

$$I(d) = \nabla_d t(d)^T \, \Sigma^{-1} \, \nabla_d t(d) \tag{2.25}$$

$\nabla_d t(d)$ is the gradient matrix of the observations vector regarding $d_i$, whereas $\Sigma$ is the covariance matrix, in which the diagonal contains the standard deviation of the components of each noise vector, construed as $(\sigma_1^2, \sigma_2^2, ..., \sigma_N^2)$ .

After formulated, the Fisher Information Matrix it will indicate the quantity of information that a certain sensor configuration can give about a position in space. Hence the goal is to obtain the maximum achievable information. By calculating the determinant of FIM it is possible to deduce the minimum *uncertainty ellipsoid* and therefore the configuration's best possible performance. Therefore, the optimal solution is given by the maximum output of the determinant of FIM.

Additionally, it is possible to detail this information by calculating the actual size of the axis that compose the *uncertainty ellipsoid*. This is achieved by calculating the square mean root of the eigenvalues of $I(d)$, which correspond to each axis size.

Further explanation about the methods used in a deeper exploration of the Crámer-Rao lower bound can be consulted in [23], which serves as guide to investigate other scenarios of application of this theorem. However, the mentioned concepts were all the necessary for the approach on this dissertation .

This same process is adopted in this dissertation. All steps specifically taken for this study are declared in section 4.2.4 of the present document.

### 2.7.2 Optimal design and optimality criteria

When contemplating system designs, the optimal solution for a problem is generally a subjective matter which depends on the chosen principal. Following this idea, we can define optimal designs as experimentally generated designs of various types of systems which are usually optimal for a targeted statistical model and are modelled by a specific optimality criterion. These criteria can be organized in four distinct groups [24]:

- **Information-based** : comprehends all criteria that are related to the Fisher information matrix $X'X$. Some of the criteria which fits into this category are A, D, E and G-optimality.

- **Distance-based** : includes criteria which depends on the distance $d(x,A)$ from a point $x$ in the Euclidean space $\mathbb{R}^p$ to a set $A \subset \mathbb{R}^p$. U and S-optimality are integrated in this category.
- **Compound design** : combine different adjusted criteria in different weighted proportions in order to meet a desired statistical function.
- Other : all criteria which do not fit in the previous three sets can be encompassed in a fourth general set.

The most relevant category for the present work is the information-based criteria, since we want to maximize the information that can be extracted from a certain design and we do not need to minimize the distances between the receptors and the source. Therefore some of the most commonly used criteria will be better explained in the following subsections.

#### 2.7.2.1 D-optimality

#### 2.7.2.2 E-optimality

#### 2.7.2.3 A-optimality

#### 2.7.2.4 G-optimality

### 2.7.3 Particle Swarm Optimization

PAPER: Optimal-receiver-config-short-baseline-localization-systems-using-particle-swarm-opt

Optimal-receiver-config-short-baseline-localization-systems-using-particle-swarm-opt : [25]

# Chapter 3

# Research Problem

This chapter intends to clarify the problem addressed by the present dissertation. Section 3.1 presents details and motive behind the research work as well as the problems it intends to solve. Having this clear, the dissertation hypothesis is stated in section 3.2 along with the research questions that are the main issues that are being explained with the present document. Lastly, the used validation methods are specified in section 3.3.

## 3.1 Problem Statement

The Ultra-Short Baseline system is among the most deployed positioning methods using underwater acoustics. There is a vast knowledge of its function and capabilities, therefore its implementation does not constitute a technological innovation nowadays. In the considered scenario, previously mentioned in chapter 1, an AUV is taking part on a long-term underwater mission in which it periodically sends known signals to the surface with a pinger. In such case, the mule AUV needs to be provided with an USBL system to receive the signal and estimate the position of the other AUV to navigate near it. The simplified communication system is illustrated in figure 3.1.

This partial USBL system was developed in previous dissertations and research work, which can be better understood in [26]. Briefly, the system consists on a transducer of four hydrophones forming a 3D array deployed on the mule AUV. The distance between AUVs is given by the cross-correlation between the received and expected signals. Since the operation frequency range is around hundreds of $kHz$, then the signal's wavelength is expected to be smaller then the hydrophones' baseline but not sufficient to accurately estimate the angle of arrival. Therefore, this measurement is intended to be refined with an additional phase difference calculation of the arriving signals to each hydrophone.

Considering that the survey AUV navigates freely trough undisclosed locations, the USBL system to be employed needs to fulfill particular requirements that common commercial solutions do not comply.

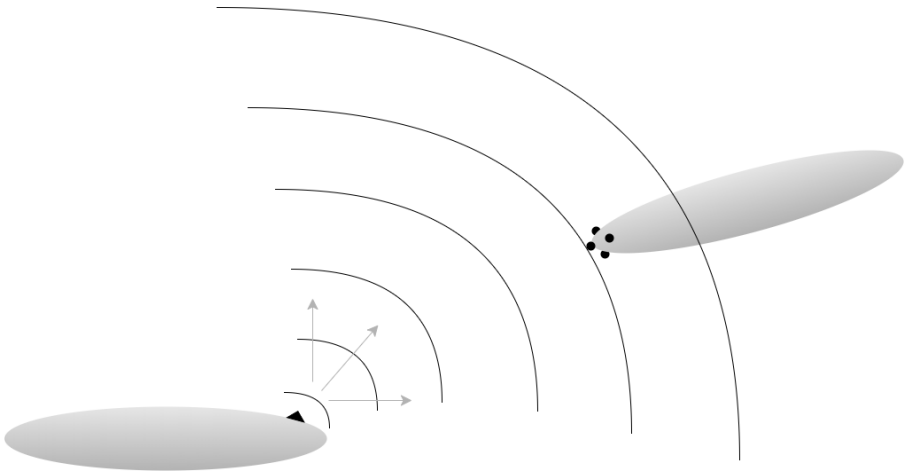

Figure 3.1: Communication System

Firstly, the system needs to be able to cover both short and long range distances, going from few centimeters to tens of kilometers between the receiver and the transmitter, with the best estimation accuracy possible. For long range positions, the accuracy of the estimation affects how direct is the path for the mule AUV to reach the acoustic source. This influences the overall resource consumption, duration of navigation search and can affect the reliability of the process. For short range position, an accurate estimate allows to avoid collisions and correctly establish chosen relative positions between vehicles. Additionally, a sampling frequency increase would also facilitate the achievement of more robust estimations. The available market systems usually offer multiple solutions with different limited operation ranges, which would force to employ more than one system to achieve the mentioned range requirement.

Secondly, the USBL system needs to be capable of detecting incoming signals from any position in space, since the localization detection is solely based on the received signals. Since the system is composed by various sensors, it is expected that they are arranged in varied positions and with different viewing angles so they can cover a wider area. However, considering they are supposed to be employed on an AUV, the vehicle's body represents an opaque obstacle to signals. Therefore, with only four fixed hydrophones, it is not possible to detect positions with full viewing angle, as intended, since not all hydrophones would have line of sight to the transmitter at all times.

The system that is proposed by this dissertation, it intended to resolve this technological gap with a system that satisfies the described requirements. Since using only four hydrophones constitutes a limitation for the viewing angle of the system, the suggested method implies deploying multiple sensors in the vehicle. From the available sensors, only four would be used simultaneously to receive the signals and feed them to the processing system. By adopting this concept, a main issue that arises is where to place the hydrophones within the vehicle. This constitutes the main research topic conducted in the present thesis.

Considering that the mentioned mechanism is meant to be applied in moving vehicles with changing environment conditions, it is useful to integrate it in a system which is responsive in real time. Accordingly, the process that selects four hydrophones among the available set

can be transformed into a dynamically reconfigurable system which enables the hydrophones commutation according to the sensors' configuration that minimizes the estimation error.

The study conducted in the scope of this dissertation intends to prove the functionality of the developed method, validate the hypothesis declared in 3.2 and draw conclusions on the research questions.

## 3.2 Hypothesis and Research Questions

This dissertation intends to complement previous research work and respond to a core research hypothesis which serves as fundamental investigation purpose. This research hypothesis can be stated as:

*"Using a USBL system which dynamically reconfigures the hydrophone selection leads to an improvement on the underwater localization accuracy, allows to have a wider viewing angle and makes it suitable for both short and long range estimation."*

Attending the proposed hypothesis, the topics that are intended to be explored and discussed in this thesis's work can be summarized in the following research questions:

- **RQ1:** *What method should be adopted in order to efficiently compare the performance of hydrophone configurations?*
- **RQ2:** *What decision metric(s) should be used to evaluate the optimal hydrophone configuration for a specific angle of arrival?*
- **RQ3:** *How should the system be developed in order to have a broad viewing angle of the space?*
- **RQ2:** *Are there distinct best hydrophone configurations for short and long range estimation?*

These questions summarize the main topic points which are explored in the scope of this thesis and are the essential inquiries that it intends to answer.

## 3.3 Validation Methods

The validation of scientific work is a key factor to demonstrate how reliable and effective it is. In this thesis, three essential methods are used to validate the functionality of the developed techniques:

- **Simulation**

  The considered immediate approach to evaluate the functionality and behavior of the system consists in creating a set of simulation procedures which are as close as possible to the real

environment and the physical system. These simulations were made as MATLAB scripts carefully designed to integrate realistic parameters, such as expected environment noise and other limitations.

- **Scientifically recognized methods**

  When composing a system, it can be useful comparing the studied approach with widely used methods which are recognized in the scientific community as robust and trustworthy. By doing this, we can gain a level of confidence in the developed system and in the obtained results.

- **Field experiments**

  After having the analytical methods and simulations coherent, it is essential then to test the system in a real environment in order to understand if the system still works correctly when real conditions are added. By testing it in a real application it is possible to take conclusions about its robustness and consider improvements or refinements for the system. In the present work, only the developed hardware design was subjected to field tests.

# Chapter 4

# Ultra-Short Baseline System

This chapter is dedicated to the presentation of the developed USBL system, which can be divided in two essential sections.

In the first part, the developed hardware module is introduced which receives acoustic signals from the hydrophones and computes the phase differences between them. The design decisions are explained along with some mathematical notions and block diagrams that represent the projected system.

In a second section, a study is conducted on three different methods in order to determine which tool is the preferred to evaluate the performance of diverse sensor configurations. First, a theoretical approach to the methods is provided followed by a functional demonstration through diverse simulation scenarios, in order to understand the behavior of the mechanisms as well as compare the performance evaluation achieved by each of them. The conclusion includes an analysis to the preferred methods for specific conditions and the overall most suitable method for the present USBL application is indicated.

## 4.1 HDL Module Architecture

The USBL system was developed in previous dissertations and research work, which can be better understood in [26]. Briefly, the system consists on a transducer of four hydrophones forming a 3D array deployed on the mule AUV. This array will receive the same signal wave front. The system then calculates the cross-correlation between the received and expected signals, which is a BPSK modulated binary sequence. The cross-correlation peak indicates the distance between AUVs and it is calculated with timing resolution corresponding to 1 sampling period of the acquired signal, which in the developed systems corresponds approximately to 6mm (with a sampling frequency of 244kHz).

Since we are referring to an USBL system and due to the limitations in dimension of the AUV that will integrate this system, the hydrophones have to be placed within a few centimeters from each other. For this reason, the obtained time resolution by using only the cross-correlation, corresponding to a maximum distance accuracy of approximately 6mm, will not be enough for

the calculation of the angle of arrival of the sound wave. Thus, in this thesis it is intended to refine this measurement by additionally calculating the phase differences of the arriving signals to each hydrophone. Upon having this measurement refined, the phase differences, as well as additional data from modules already implemented, will serve as input in a software mechanism that estimates the angle of arrival of the received signal to the hydrophone array.

The proposed module receives 4 inputs, which correspond to the received signals in each hydrophone, and outputs the average phase difference between all combinations of hydrophone pairs. This model was developed using Verilog, which is a commonly used hardware description language, and all designed components were validated with testbenches through simulations.

The module is a synchronous system, since all elements are synchronized by a global clock. It follows a sequential logic, so it is time dependent and contains memory elements. All sub components receive an input from a memory element triggered by the clock and originates an output which is also saved in a memory element triggered by the clock, in order to avoid capturing unstable signals.

### 4.1.1 Module components

The overall system is composed by four main functional blocks, represented in 4.1. The hydrophone array, composed by hydrophones $i$ with $i = \{1,2,3,4\}$, receives the signals in each sensor and sends them to an Analog to Digital Converter (ADC). The generated digital signals are then input of a module based on a Hilbert transform, which converts the real signal to a complex representation. These are then multiplexed so each pair of real, $Re_i$, and imaginary, $Im_i$, components are input in a CORDIC [27] block, responsible for computing the signal's phase, $phase_i$. Afterwards, it is possible to calculate the phase differences for all combinations of pairs, $diff_{ij}$ with $i \neq j$, which are finally averaged in order to obtain a more stable phase difference, $\Delta phase_{ij}$.

The module receives a global clock and reset which are connected to all registers, as well as an enable signal which allows the sub modules to capture new inputs and release the outputs synchronically.

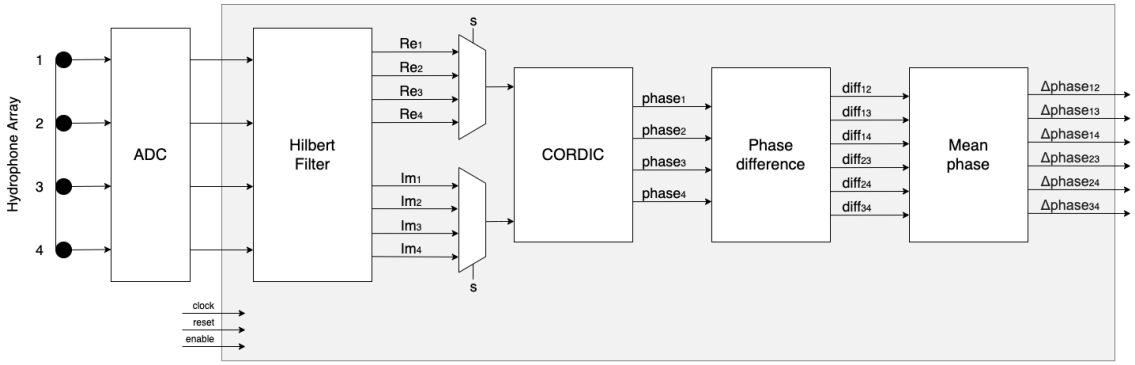


Figure 4.1: Top level architecture

Considering that the ADC receives signals at a frequency of $244kHz$ and outputs at a frequency of $125MHz$, then the system received a new input every 512 clock cycles. Assuming that a latency of a few inputs is tolerable, then each sub component can use up to 512 clock cycles since receiving an input until generating an output. As the performed calculations are fairly simple, the available clock cycles are more than enough to originate the outputs, therefore this architecture does not involve time constraints. Instead, it focuses on minimizing the used area since it is part of a complex system that already uses a substantial part of the FPGA resources.

In order to describe the efforts to minimize the used area, all module sub components are detailed next, namely the Hilbert filter, CORDIC, Phase difference and Mean phase.

#### 4.1.1.1 Hilbert Filter

The signals coming from the ADC are purely real so they need to be converted to their analytic representation. This is achieved by using a module based on a Hilbert FIR filter, which derives the complex representation by comprehending the original real signal and its Hilbert transform.

The Hilbert transform definition is given by 4.1 [**?**], where $x(t)$ is the original signal and $P$ is the Cauchy principal value.

$$H(x)(t) = \frac{1}{\pi} P \int_{-\infty}^{\infty} \frac{x(\tau)}{t-\tau} d\tau \tag{4.1}$$

The notation for a digital N-th order FIR filter can be expressed by equation 1 in [28]. Assuming a eighth-order filter that can be approximated with alternated zero coefficients, then equation 4.3 represents the imaginary part of the signal, $Imag_0$, for a sample $x_0$ received in the present moment , assuming $x_{-i}$ as the input samples received $i$ sampling periods before. Then, 4.3 represents the real part of the signal for the same sample, which simply consists on delaying four sampling periods the original signal.

$$Imag_0 = a_1\, x_{-1} + a_3\, x_{-3} + a_5\, x_{-5} + a_7\, x_{-7} \tag{4.2}$$

$$Real_0 = x_{-4} \tag{4.3}$$

The eighth-order coefficients can be obtained through a design tool, such as the *designfilt* function on MATLAB, and respect an odd anti-symmetry, i.e. $a_1 = -a_7$ and $a_3 = -a_5$.

In order to implement this filter, the most common approach is to use a chain of registers that integrate multiple adders and multipliers, so that the calculations take less clock cycles to obtain a valid result, similarly to the work in [28]. However, since the goal of this implementation is to minimize area, then an alternative approach was formulated which uses only one multiplier and one adder. As can be observed in the filter equation, all odd samples need to be multiplied by a coefficient and summed with each other. Therefore, by using a circular shifting register chain 4.2

for each arriving signal, it is possible to position each of the buffer chain's samples in register $x_8$, which is used for external calculations.

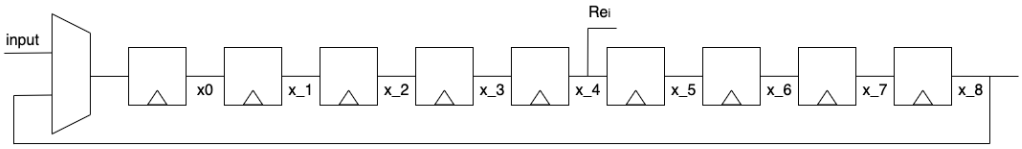


Figure 4.2: Hilbert Filter circular shifting register chain

In a more comprehensive view, the register chains $HF_{Ci}$ are integrated with the remaining block elements as represented in 4.3. The module receives four signals as input and outputs the real and imaginary components, $Real_i$ and $Imag_i$, for each of them.

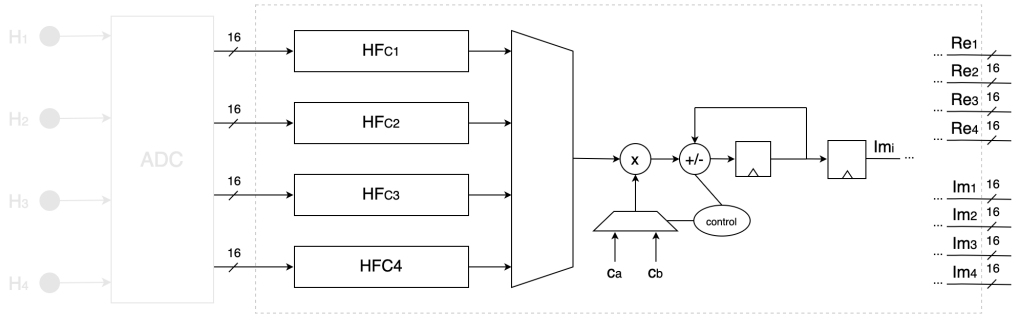


Figure 4.3: Hilbert Filter block diagram

The implementation contains a series of design decisions that lead to decreased area occupation, presented as follows :

- The four register chains are multiplexed so that the module needs only one multiplier and one adder to calculate the Hilbert transform for all signals;
- Since the coefficients have odd symmetric pairs, then only two variables and their symmetric value are needed, which will be referred as $c_a$, $c_b$, -$c_a$ and -$c_b$. For even samples, associated with coefficients equal to zero, a controller unit is responsible for skipping the multiplication, which saves energy. For odd samples, the control unit alternates between the positive and negative coefficients to be multiplied. The control unit settings are summarized in table 4.1 for each register chain sample.
- The negative coefficients are achieved by subtracting the result of $a_i\ x_{-i}$, i.e. negating the adder, so only one adder block is necessary;
- A register is placed after the adder so that it interactively accumulates the value that is correspondent to the imaginary component $Im_i$ after the full chain circle shifting.

Having cleared the implementation details, it is possible to deduce that each $HF_{Ci}$ takes 9 clock cycles to be processed. Therefore, the entire calculation takes $9 \times 4$ clock cycles plus one additional cycle to update the outputs.

| | Multiplier Coefficient | Adder mode |
|---|---|---|
| $a_0$ | 0 | - |
| $a_1$ | -$c_a$ | - |
| $a_2$ | 0 | - |
| $a_3$ | -$c_b$ | - |
| $a_4$ | 0 | + |
| $a_5$ | $c_b$ | + |
| $a_6$ | 0 | + |
| $a_7$ | $c_a$ | + |
| $a_8$ | 0 | + |

Table 4.1: Hilbert filter control unit settings for each processed sample

An additional detail can be pointed out regarding the impulse response of the Hilbert filter. For high filter orders, the impulse response does not suffer substantial attenuation. However, for an eighth-order filter there is a visible gain attenuation and overflow, which leads to wrong results if the dynamic range is not adequate. Therefore, it is possible to create a mechanism that applies variable gain to the filter output depending on the frequency so that it is possible to make it constant and avoid this issue.

#### 4.1.1.2 CORDIC

The CORDIC algorithm is used for real-time trigonometric and exponential calculations, as well as polar to rectangular conversions and vice-versa, using iterative vector rotations.

The implemented CORDIC module has a sequential structure, as it occupies the least area, and it is responsible for receiving the real and imaginary components of a signal and outputting its phase. There are two possible modes of operation from which it is used the vectoring mode (VM), whose algorithm computes the magnitude and phase of the input vector $((x_0, y_0))$ from the x-axis [27]. This is achieved by iteratively approximating the phase through angle microrotations of $\alpha_i = \pm atan(2^{-i})$ which are summed originating an approximated phase. The result is given in a 16 bit value, which is composed by 9 bits for the integer part and 7 bits that represent the fractional portion.

The CORDIC iterations are expressed by 4.4, 4.5 and 4.6 for $d_i$ belonging to {-1,1}.

$$x_{i+1} = x_i - d_i \, 2^{-1} \, y_i \tag{4.4}$$

$$y_{i+1} = y_i + d_i \, 2^{-1} \, x_i \tag{4.5}$$

$$z_{i+1} = z_i - d_i \, \alpha_i \tag{4.6}$$

The CORDIC logic uses a 16 element ROM (Read-Only Memory) that stores the $atan(2^{-1})$ values required for the algorithm. Additionally, another sub component provides a binary counter that defines the number of performed iterations and it is also responsible for generating the address to access the ROM.

Considering that the CORDIC module uses 16 clock cycles to run through the entire ROM and one additional cycle to update the outputs, there are still many remaining clock cycles from the 512 available. Therefore, the design uses only one CORDIC module with multiplexed inputs so the process takes $17 \times 4$ plus one, to update the global outputs, in a total of 69 clock cycles.

#### 4.1.1.3 Phase difference

This sub module is responsible for computing the phase differences between the previously determined signals' phases, $phase_i$. For four inputs $phase_i$, it is generated the difference between all combinations of hydrophones, resulting in six pairs: 12, 13, 14, 23, 24 and 34.

This is achieved using a single subtractor which has multiplexed inputs so that the calculations can be executed within the 512 clock cycles with only one block of hardware, instead of dedicated subtractor for each calculation.

The result is given in a 16 bit value, which is composed by 10 bits for the integer part and 6 bits that represent the fractional portion.

#### 4.1.1.4 Mean phase

Finally, the last sub module is responsible for accumulating N samples of the phase difference $diff_{ij}$ and calculate a mean phase difference, so that the value is less affected by variations. Parameter N depends on a customizable input $k$ where $2^k = N$.

The averaged phase differences is given in a 16 bit value, which is composed by 10 bits for the integer part and 6 bits that represent the fractional portion.

### 4.1.2 Performance and resource analysis

The module that computed the phase differences is intended to decrease the used area, thus the used components, in order to improve an existing version of a design with the same purpose. The previous version used approximately 10k slice registers and 6k slice LUTs, whereas the present architecture reduced these numbers to 1216 and 1432, respectively, consisting of a successful improvement.

This module was integrated in the global complex system which was subjected to field tests in the water. Although the ground truth was not rigorous, after processing the results, it was roughly estimated that the phase differences do not vary more than 15°, which corresponds to approximately $2.5mm$. Comparatively to the previous $6mm$ of time resolution achieved through correlation, this result constitutes an improvement. Therefore, after this initial analysis, it is considered that the process which uses the phase differences along with the correlation is expected to improve the angle of arrival estimation precision.

## 4.2 Methods for configuration performance evaluation

As previously declared, the present dissertation ultimately intends to develop a reliable method that determines the optimal configuration to minimize the estimation error. For this purpose, it is necessary to employ a complementary mechanism which is able to perform experiments on sensor configurations in order to quantify their performance based on chosen decision parameters.

Therefore, three different methods will be presented in this section as potential tools to be used. Firstly, a theoretical approach will be detailed, followed by a functional exemplification of each process. Lastly, a practical comparison between them will be presented in order to disclose the preferred option for this application.

The chosen methods are a Monte Carlo estimator based on TDoA, a Monte Carlo estimator based on a plane wavefront and the Fisher Information Matrix.

### 4.2.1 Preliminary considerations

In order to better understand the used mechanisms for estimating positions, some preliminary considerations are laid out. These contemplate system definitions, deductions about system's phenomena and considered approximations. The following topics are discussed:

- the number of used sensors for the estimation;
- a phase ambiguity issue that affects the ToA determination;
- the relation between the phase differences of hydrophones in known relative positions and the possible location of the transmitter;
- an approximation used for the ToA measurement;
- the influence of the Doppler effect in the system.

#### 4.2.1.1 Number of sensors

For the estimation of the position in 3D space, a multilateration approach was used. As explained in 2.3.3, the concept of multilateration combines the information of the relative distances between multiple sensors and a target in order to locate it.

In the present case, a total of four sensors are needed so that it is possible to define the position of target. Using only two sensors, two possibility spheres are formed around these sensors whose intersection originates a circle that contains the location possible solutions. By adding a third sensor, this circle is intersected by another sphere which originates only two location possibilities. Finally, a fourth sensor is added so that it is possible to exactly differentiate which one of the two final solutions is the accurate location solution.

#### 4.2.1.2 Phase Ambiguity

When the information about the time of arrival of a signal is available, it is relatively easy to estimate the range of the communication since there can be a direct conversion between them. However, when dealing with phase differences, there is no exact time notion, so it is necessary to start by defining a reference point.

Considering sinusoidal signals, when we have an array with four hydrophones spatially placed to form a 3D layout, the signal that is arriving to each hydrophone in different times consequently have different phases. However, since sinusoidal signals are periodic, this means that for different signal periods the same phase value is observed, i.e. the phase is ambiguous. It is possible to observe this phenomenon in figure 4.4. In this illustration, $\alpha$ represents the observable phase difference of hydrophone $H_4$ to the reference point $H_1$. However, the actual phase difference which is intended to obtain, $\Delta p_4$, is one period of the signal, $\lambda$, added to the observable phase $\alpha$.

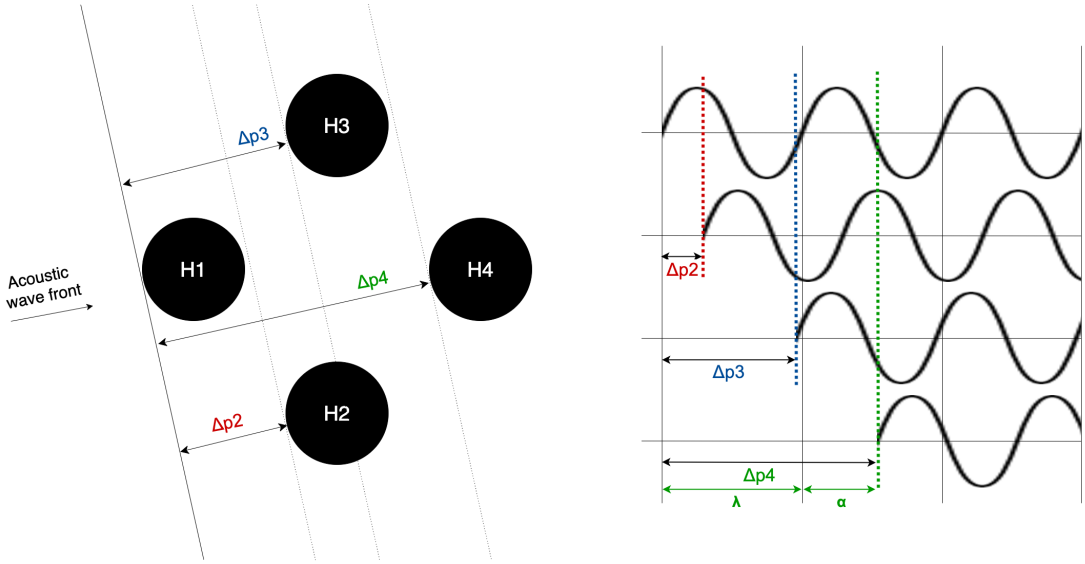


Figure 4.4: Phase difference to reference point and phase ambiguity

For this reason, it is crucial to consider that the phase difference is given by the obtained phase value added by the number of periods ahead from the considered reference period.

In the system under study, the sent signals work with a operation frequency of 24.4 $kHz$. The corresponding signal period is $T = \frac{1}{24400}$ seconds which, considering the underwater acoustic speed $c$ equal to a standard 1500 $m/s$, the wavelength is approximately equal to $\lambda = \frac{T}{c} = 6.1cm$. Having this into consideration, after obtaining the time of arrival to each hydrophone given by the cross correlation instances, besides the reference one, it is possible to conclude if the phase shift is superior to one period by analyzing if the time difference is greater than the duration of one period $T$. In figure 4.4, each mentioned time difference between $H_1$ and $H_2$, $H_3$ and $H_4$ is converted to the corresponding phase differences $\Delta p_2$, $\Delta p_3$ and $\Delta p_4$.

One possibility to solve phase ambiguity in this system would be to place the four hydrophones with a baseline spacing inferior to $\frac{1}{2}$ of a wavelength, since the maximum reached

by phase difference is 180 degrees. This way it would be possible to immediately deduce the phase difference since it would always be contained in one period. However, positioning the hydrophones closer together leads to smaller values,causing a consequent increase on the estimation error due to varying environment conditions (briefly enumerated in 2.1). Additionally, since the hydrophones to be used in this system have a corresponding diameter of roughly half of a wavelength, they would not allow to execute the mentioned configuration and so this possibility will not be contemplated.

In order to compensate this phase ambiguity, a simple relation was developed which allows to calculate the absolute time difference between the moment a signal is received by hydrophone A, $T_A$, and when the same signal is received by a further hydrophone B, $T_B$. Figure 4.5 illustrates this association, where the represented sinusoidal waves correspond to the same signal arriving at hydrophones A and B. This correspondence uses the time stamps obtained by the correlation peaks combined with the calculated phase difference, that is determined in parallel, so that the measurement is more accurate. Equation 4.7 translates this relation, where $t_1$ and $t_2$ are the correlation peaks obtained from the signal arriving at hydrophone A and B, respectively, and so by rounding for the next integer number the difference between the correlation peaks, $t_2 - t_1$, we will obtain in which period, $T$, of signal in A will the signal in B arrive. Then the measurement is improved by subtracting a phase difference, $\theta_B - \theta_A$, so that the instant in which the signal is detected in hydrophone B can be defined.

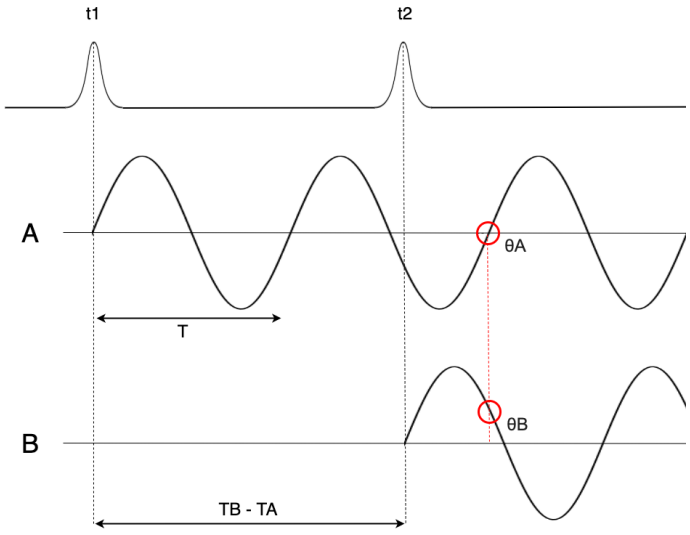


Figure 4.5: Ambiguity correction through correlation and phase difference

$$T_B - T_A = round(\tfrac{t_2 - t_1}{T}) - (\theta_B - \theta_A) \tag{4.7}$$

#### 4.2.1.3 Hydrophone position in relation to ToA

To better understand the location estimation of an acoustic source in relation to the position of a pair of hydrophones, we can initially adopt the two dimensional scenario of figure 4.6.

Considering two hydrophones at known relative positions $(-f,0)$ and $(f,0)$, we can model all possible acoustic source locations for a specific ToA through hyperbolas. This is due to the fact that, by definition, the sum of the distances from the focus of each hyperbole, where each hydrophone is placed, to any point of the hyperbolic geometry corresponds to a constant value. This means that, in figure 4.6, any point $(x,y)$ that is contained in the hyperbole corresponds to a constant $|d_2 - d_1|$ value which, after some formulation, is in fact equal to $2 * v$ or the distance between the vertexes of each hydrophone's hyperbola. Therefore, it is possible to trace a hyperbole that represents the positions of the target in space both based on their distance and the signal's ToA. In the exceptional case where $d_3 = d_4$, we can observe that the possible positions are represented by an equidistant straight line to each hydrophone, such as the y axis.

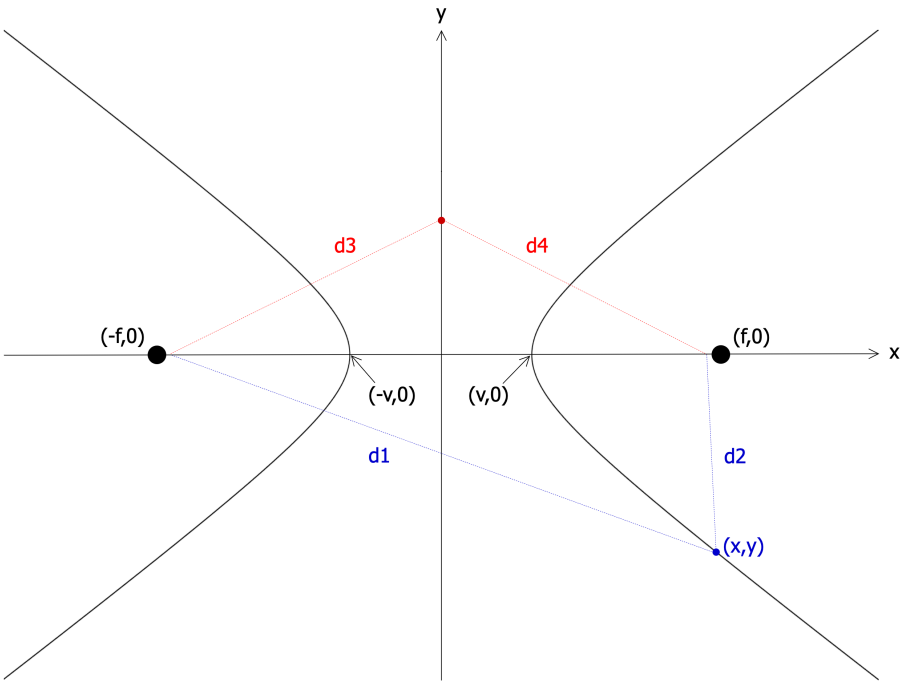


Figure 4.6: Hyperbolic representation of acoustic source position possibilities in relation to ToA to two hydrophones

#### 4.2.1.4 ToA approximation

In order to estimate the location of an acoustic source we take into account the phase differences between each pair of hydrophones, carefully explained in section 4.1. These phase differences can be translated into periods of the signal which combined with the ToA obtained from correlation of arriving acoustic signals are equivalent to relative distances.

Following the previous idea, it is possible to model the distance of one sensor to the target based on the known distance of a second sensor to the same target. This is to say that for two sensors with known relative positions where hydrophone 1 is the closer to the target, the distance from hydrophone i to the target, $D_i$, can be expressed as the distance of hydrophone j to the target, $D_j$, added by the time difference of arrival, $\Delta t_{ij}$, multiplied by the propagation velocity, $c_s$. Overall, this relationship is declared in equation 4.8.

$$D_i = D_j + \Delta t_{ij} * c_s \tag{4.8}$$

Therefore, the same logic can be applied for multiple hydrophones. In the present work, in which it is considered a system with four hydrophones, a synchronization mechanism allows to determine the signals' ToA between the transceiver and the hydrophones. However, in order to simplify the synchronicity and decrease errors that arise from it, the module that precisely computes the phase differences of the received signal in the hydrophones is used so that is possible to apply the relationship in 4.8. Consequently, a better angle of arrival estimation can be achieved when using this approximation than if all four times of arrival are used for the same purpose.

#### 4.2.1.5 Doppler Effect

The implemented process uses the information of the transmitted signal's operating frequency in order to compute the phase differences and determine the overall times of arrival. However, in real scenarios the environmental conditions can distort this frequency between the source and the receiver. In the present study, since the vehicle is predominantly moving, then the Doppler effect could influence the signal's frequency, leading to erroneous calculations.

In order to evaluate if the Doppler effect influences the system, it is possible to calculate which is be the frequency deviation observed for a known relative speed between vehicles. Considering that the relative speed between the transmitter and the receiver is denoted as *relative_speed* and using a fixed sound speed, $c_s$, with a determined frequency of the transmitted signal, the relation 4.9 can be established.

$$freq\_deviation = \frac{relative\_speed}{c_s} \times signal\_freq \tag{4.9}$$

Therefore, considering the frequency of the signal equal to $24.4kHz$ and a $c_s$ of $1500m/s$, it is observable that the frequency deviation will be dependent on the relative speed. Considering a transmitter that is static and a typical value for the navigation velocity of an AUV around $2m/s$, which results in a frequency deviation of approximately $32.5Hz$. This allows to consider the Doppler effect negligible in this case.

A way to prevent this deviation is to integrate a frequency detector which senses the relative navigation speed in real time and adapts the used frequency. This mechanism is not integrated in the present research work.

### 4.2.2 Monte Carlo estimator based on TDoA

The goal of the first proposed method is to estimate the position of an acoustic source in relation to known positions of a configuration of sensors, in a system of geometric axes with a defined origin. For this purpose, the logic employed is based on vector algebra with other physical considerations, detailed in the present subsection.

Figure 4.7 represents the schematic of a considered scenario, where four hydrophones are placed in known relative positions in space and the origin of the axis is set on the body of the AUV or an alternative fixed structure. Then $r_i$ is defined as the vector that connects the origin of the axis to hydrophone $i$ and $rr_i$ defines the vector that connects hydrophone $i$ to the acoustic source. The black cross represents the acoustic source which is located somewhere in space. At last, the subtraction of the mentioned vectors is equal to $r$, according to 4.10, which corresponds to the position of the acoustic source in relation to the origin of the axis and, overall, it is the variable that the method aims to determine.

$$r_i = r + rr_i \tag{4.10}$$

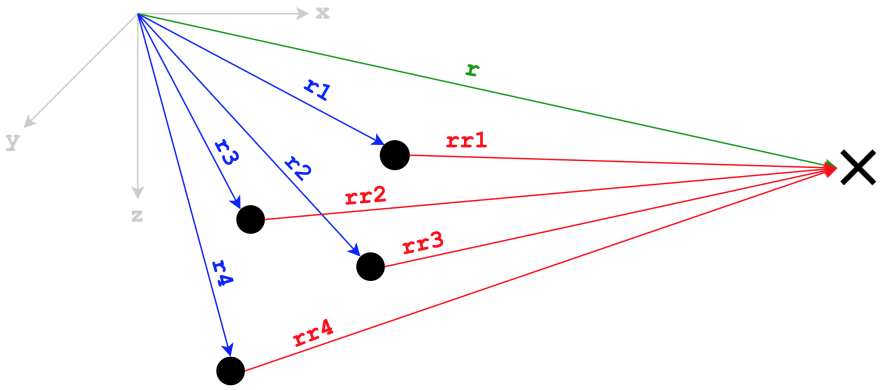


Figure 4.7: Considered scheme for angle of arrival estimation

Then we can define the times of arrival to each hydrophone as 4.11, where $t_0$ is the absolute time of emission, $c_s$ is the underwater sound speed and $\rho_i$ is the norm of $rr_i$, 4.15, which translates to the distance from hydrophone $i$ to the acoustic source.

$$t_i = t_0 + \frac{\rho_i}{c_s} \tag{4.11}$$

However, as explained previously, instead of using the absolute ToA in each hydrophone by computing the expression 4.11 for each of them, it can be expressed as a function of a single reference ToA. A simple logic was applied in order to determine this reference hydrophone, which starts by identifying the closest to the acoustic source. This allows to obtain all relative times of arrival by adding the defined reference time to each between a hydrophone and the reference one. This is achieved by analyzing the of each pair, $\Delta t_{ij}$, for all possible combinations of two among four hydrophones, making up a total of six combinations. Considering each hydrophone pair $ij$ with $i, j = \{1,2,3,4\}$ :

- if $\Delta t_{ij}$ is positive, then hydrophone $i$ is closer to the acoustic source
- if $\Delta t_{ij}$ is negative, then hydrophone $j$ is closer to the acoustic source
- if $\Delta t_{ij}$ is zero, then $i$ and $j$ hydrophones are equidistant to the acoustic source

Considering these relations, it is possible to compose a vector that accumulates the closer hydrophone between each pair for a certain position of the acoustic source. Extracting the mode of this vector will then return the chosen hydrophone in most cases and therefore the overall closer to the acoustic source. If the closer hydrophones are the equidistant to the source, then it is indifferent which one is selected.

Thereafter, recalling expression 4.8, it is possible to write 4.12, 4.13 and 4.14 which translate the used relations, where the chose reference sensor is hydrophone 1, for the purpose of exemplification.

$$T_2 = T_1 + \Delta t_{12} * c_s \tag{4.12}$$

$$T_3 = T_1 + \Delta t_{13} * c_s \tag{4.13}$$

$$T_4 = T_1 + \Delta t_{14} * c_s \tag{4.14}$$

If then the distance $\rho_i$ is raised to the power of two, we know that $||rr_i||^2 = r_i^T r_i$, which allows to deduce equation 4.16 after some mathematical manipulation. Considering $\rho_i$ a physical distance, it is also possible to express it trough equation 4.17, which uses the speed of propagation underwater multiplied by the ToA of the signal from the acoustic source to hydrophone $i$.

$$\rho_i = ||rr_i|| \tag{4.15}$$

$$\rho_i^2 = r^T r + 2r^T r_i + r_i^T r_i \tag{4.16}$$

$$\rho_i^2 = c_s^2 (t_i - t_0)^2 \tag{4.17}$$

Since two distinct relations are defined for $\rho_i^2$, then it is possible to consider the algebraic expressions as equivalent, thus forming a single equation to be resolved with only one unknown

variable. After some mathematical manipulation, the matrix relation 4.18 is achieved, where $r$ is isolated and can be estimated.

$$\begin{bmatrix} 1 & 2\,r_i^T \end{bmatrix} \begin{bmatrix} r^T r \\ r \end{bmatrix} = \begin{bmatrix} c_s^2(t_i - t_0) - r_i^T r_i \end{bmatrix} \tag{4.18}$$

In order to resolve this system of equations and isolate $r$, the least squares method is applied. If 4.18 is extended to the four considered hydrophones, we obtain matrix $A$ represented as 4.19 and $Y$ equivalent to 4.20. It is important to notice that the $A$ matrix has to be invertible, thus the rows which contain the chosen hydrophone configuration have to be linearly independent. The least squares method is then expressed as 4.21, where $X \in \mathbb{R}^4$ holds the Cartesian result of $r$. As the method formulates four equations that are meant to calculate only three coordinates, $X$ will contain a fourth element that consists on a nonlinear component equivalent to $||r||^2$.

$$A = \begin{bmatrix} 1 & 2\,r_1^T \\ 1 & 2\,r_2^T \\ 1 & 2\,r_3^T \\ 1 & 2\,r_4^T \end{bmatrix} \tag{4.19}$$

$$Y = \begin{bmatrix} c_s^2\,(t_1 - t_0)^2 - r_1^T r_1 \\ c_s^2\,(t_2 - t_0)^2 - r_2^T r_2 \\ c_s^2\,(t_3 - t_0)^2 - r_3^T r_3 \\ c_s^2\,(t_4 - t_0)^2 - r_4^T r_4 \end{bmatrix} \tag{4.20}$$

$$X = (A^T * A)^{-1} * A^T * Y \tag{4.21}$$

After inferring the Euclidean vector $r$, it is possible to obtain both the bearing trough its direction, $\hat{r}$, and the range through its magnitude, $||r||$.

### 4.2.3 Monte Carlo estimator based on a plane wavefront

The second explored method for evaluating sensor configurations' performance is a simpler approach than the previously proposed. It consists on an estimator which assumes that the signals' propagation can be approximated by a plane wavefront. When considering a planar wavefront approximation, it is assumed that the acoustic source is at a distance which is sufficiently larger than the relative distances between the hydrophones, for the signal to be considered to have a planar wavefront, thus the angle of arrival to each hydrophone being the same. This estimator

is posteriorly integrated in a Monte Carlo approach to evaluate the configurations based on the obtained variance given different acoustic source positions.

Using a plane wavefront approximation means that, for signals arriving to the USBL system, it is assumed that the wavefront is coincident with a plane perpendicular to the direction of propagation, thus perpendicular to the angle of arrival as well. Figure 4.8 is illustrative of a plane wavefront arriving at two sensors. As represented, the angle or arrival is considered the same for every sensor, since the wavefront is the same as well, and it is possible to deduce the time of arrival to an hydrophone 1 by using the ToA to hydrophone 2 added by the time difference of arrival between 1 and 2. Therefore, it is also possible to obtain the estimation of the range, as it will be presented next.

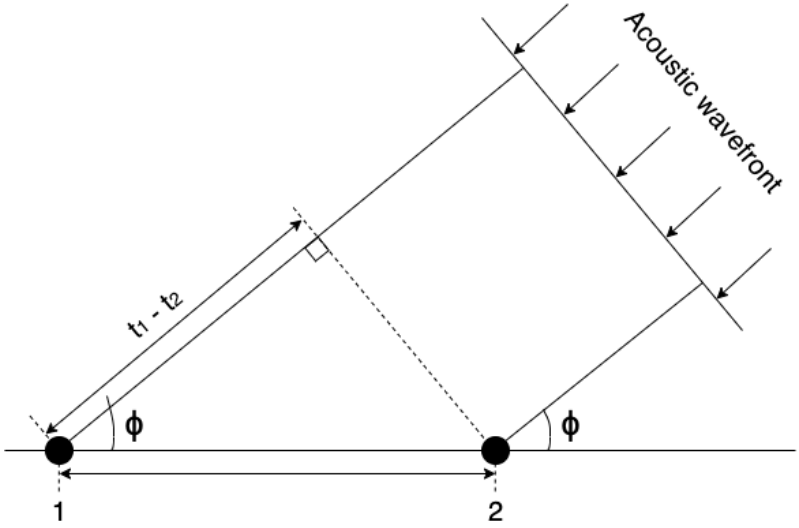


Figure 4.8: Angle of arrival relation considering a plane wavefront

The estimator considers a USBL system composed by four sensors whose positions are previously defined. The time of arrival, $t_i$, to each hydrophone, $i$, is represented by expression 4.22. The considered $t_0$ is the absolute time of emission of the signal, which is acquired through a synchronization mechanism, the $s$ is the position of the transmitter, $a$ is referent to the mass center of the USBL's position, $r_i$ is the Cartesian coordinates of the hydrophone's position, $c_s$ is the sound speed and $e_i$ is an injected error that have the same characteristics expressed previously in **??**.

$$t_i = t_0 + \frac{||s(a-r_i)||}{c_s} + e_i \tag{4.22}$$

Due to the considered approximation to the plane wavefront, it is possible to calculate the range estimation, $\rho$, as a mean all propagation times multiplied by the sound speed,$c_s$, as in equation 4.23. The $N$ represents the number of hydrophones.

$$\rho = c_s \frac{1}{N} \sum_{i=1}^{N} t_i - t_0 \tag{4.23}$$

Then a matrix $S$ is formulated as 4.24, whose rows are the difference between the position of hydrophone 1 and the remaining three, and a $\Delta$ vector is expressed as 4.25, containing all combinations of TDOA between hydrophone 1 and the remaining.

$$S = \begin{bmatrix} r_1 - r_2 \\ r_1 - r_3 \\ r_1 - r_4 \end{bmatrix} \tag{4.24}$$

$$\Delta = \begin{bmatrix} t_1 - t_2 \\ t_1 - t_3 \\ t_1 - t_4 \end{bmatrix} \tag{4.25}$$

Taking into account the defined $S$ and $\Delta$, the signal's angle of arrival can be calculated from the direction of the signal, $d$, obtained from the least squares expression 4.26 [29]. Since there are only three equations to estimate three coordinates, then the expression is linear.

$$d = c_s \left(S^T S\right)^{-1} S^T \Delta \tag{4.26}$$

Having calculated the range $\rho$ and the direction $d$, the estimate of the transmitter position is given by the multiplication of these variables.

Finally, the plane wavefront estimator was integrated in a Monte Carlo method in order to execute multiple estimations of various transmitter positions, $s$, for a specific sensor configuration, so that it is possible to draw conclusions on its performance.

### 4.2.4 Fisher Information Matrix

The Fisher Information Matrix (FIM) serves to quantify the information that an observable variable is capable of returning to an estimator. This concept is then integrated in the Crámer-Rao lower bound, which is a method that expresses the variance lower bound that a sensor configuration is capable of achieving. Unlike the two previously presented processes, the Crámer-Rao bound is independent from the used estimator, as it assumes a linear estimator that is efficient and unbiased.

The fundamental thought process and mathematical notation previously used in 2.7.1 are applied in the procedure that will be explained next.

The implementation of the Crámer-Rao bound method can be essentially partitioned in four steps:

1. Formulate the observations vector
2. Calculate the Fisher Information Matrix (FIM)
3. Calculate the determinant of FIM
4. Apply optimality criteria to draw conclusions

In this thesis, the number of used hydrophones per estimation is four, so all expressions will be presented for this case.

Firstly, the observation vectors are formulated based on an initial time of arrival $t_0$, which is given by a synchrony mechanism integrated in the global communication system, and the time of arrival based on the vectors that connect the hydrophone positions, $r_i$, to the transmitter, $s$. For a more realistic approach, it is also considered an added noise component that can be approximated to a Gaussian distribution $n_i \sim \mathcal{N}(\mu, \sigma^2)$.

The four observations vectors are then expressed as 4.27 to 4.30.

$$t_1 = t_0 + \frac{s - r_1}{c} + n_1 \tag{4.27}$$

$$t_2 = t_0 + \frac{s - r_2}{c} + n_2 \tag{4.28}$$

$$t_3 = t_0 + \frac{s - r_3}{c} + n_3 \tag{4.29}$$

$$t_4 = t_0 + \frac{s - r_4}{c} + n_4 \tag{4.30}$$

Then, addressing the second step, all conditions are set to calculate the FIM, $I(d) \in \mathbb{R}^{3x3}$. In order to do so, if $d_i = ||s - r_i||$ is the distance between each sensor and the source, the gradient of the observations vector can be expressed as shown in 4.31.

$$\nabla_d t(d) = \frac{1}{c} \begin{bmatrix} \frac{d_1^T}{||d_1||} \\ \frac{d_2^T}{||d_2||} \\ \vdots \\ \frac{d_N^T}{||d_N||} \end{bmatrix} \tag{4.31}$$

Additionally, the added noise component is present in the covariance matrix, represented as 4.32, which integrates the FIM equation.

$$\Sigma = \begin{bmatrix} \sigma_1^2 & 0 & 0 & 0 \\ 0 & \sigma_2^2 & 0 & 0 \\ 0 & 0 & \sigma_3^2 & 0 \\ 0 & 0 & 0 & \sigma_4^2 \end{bmatrix} \tag{4.32}$$

Overall, the conditions to obtain the FIM matrix are established and, after some mathematical formulation, it can be expressed as 4.33. This function can be validated by a similar study made on TOA based optimal positioning [30].

$$I(d) = \frac{1}{c^2}\left[\sum_{n=1}^{N} \frac{d_i d_i^T}{||d_i||^2} \frac{1}{\sigma_i^2}\right] \tag{4.33}$$

The final step is to calculate the determinant and find its relation to the volume of the *uncertainty ellipsoid*. As mentioned before, in 2.7.1, the Fisher Information Matrix determinant returns a deterministic value that represents the quantity of information which can be obtained and, therefore, the objective is to maximize it by respecting the condition $argmax\, det(I(d))$.

#### 4.2.4.1 Optimality criteria

In order to evaluate the obtained values, several different optimality criteria can be applied. Considering similar applications in literature, the criterion that the most relevant for the present case is the E-optimality, which minimizes the largest eigenvalue of the inverted FIM.

The FIM can be associated with a physical meaning, more specifically an uncertainty volume that characterizes the variance that a specific configuration can achieve for an estimate. In an initial approach the ellipsoid was not considered and instead an uncertainty sphere was analyzed. The radius of the uncertainty sphere, $u_{sphere}$, is expressed as 4.34, which relates the three ellipsoid axis into a single mean radius that originates a figure of the same volume.

$$u_{sphere}(d) = \sqrt[2]{\sqrt[3]{det(I(d)^{-1})}} \tag{4.34}$$

In this situation, the optimization objective is expressed as $argminu_{sphere}(d)$, which indicates that the error that originates a certain uncertainty radius is minimal.

In a further analysis, the uncertainty ellipsoid is calculated using 4.35. The squared eigenvalues of the inverse of the FIM indicate the length of each of the three ellipsoid axis and the eigenvectors specify the direction of each axis. An eigenvector that is associated with the smaller eigenvalue indicates the direction in which there is less uncertainty and, equivalently, an eigenvector whose eigenvalue is the larger represents the direction in which there is the biggest uncertainty. Consequently, the goal in this case is to minimize the maximum squared eigenvalue of the FIM inverse, $argmin\, max(\sqrt{eigenvalue})$.

$$u_{ellipsoid}(d) = \sqrt[2]{eig(I(d)^{-1})} \tag{4.35}$$

Besides the E-optimality, several more criteria can be used in order to evaluate the performance of a specific hydrophone configuration, using the Fisher Information Matrix. The most common alternatives would be:

- A-optimality: minimizes the trace of the inverse of the FIM, therefore seeks the minimum average variance of the estimates.
- D-optimality: minimizes the determinant of the inverse of the FIM, therefore the volume of the uncertainty sphere. However, this can be misleading since the information obtained for one direction can be much larger than the other directions, constituting a large FIM determinant which is not representative of the full estimation.

### 4.2.5 Performance comparison between methods

Upon presenting the theoretical details behind the three considered methods for evaluating configurations' performance, a further functional study will be presented through simulation results.

Throughout the functional demonstrations, three different hydrophone configurations are considered, A, B and C defined in 4.2, where the columns $r_{Ai}$, $r_{Bi}$ and $r_{Ci}$ contain the position's coordinates of each hydrophone $i$.

| | $r_{A1}$ | $r_{A2}$ | $r_{A3}$ | $r_{A4}$ | $r_{B1}$ | $r_{B2}$ | $r_{B3}$ | $r_{B4}$ | $r_{C1}$ | $r_{C2}$ | $r_{C3}$ | $r_{C4}$ |
|---|---|---|---|---|---|---|---|---|---|---|---|---|
| x | 0.02 | 0.02 | 0 | 0 | 0.1 | 0.1 | 0 | 0 | 0.1 | 0 | 0 | 0 |
| y | 0 | 0 | 0.1 | -0.1 | 0 | 0 | 0.1 | -0.1 | 0 | 0 | -0.0707 | 0.0707 |
| z | 0.1 | -0.1 | 0 | 0 | 0.1 | -0.1 | 0 | 0 | 0 | 0.1 | -0.0707 | -0.0707 |

Table 4.2: Hydrophone configurations used for accuracy tests

For testing both estimators, a methodology was formulated in order to evaluate the accuracy that they can achieve in defined circumstances. This approach is a Monte Carlo algorithm which allows to reiterate the estimation process according to the number of positions that are intended to be tested for a specific configuration, as well as create a series of repetitive calculations that allow to deduce the estimation error and turn the overall process more robust. For this initial study, the following conditions are considered:

a) **Sensor Configuration**

Each hydrophone configuration is analyzed individually. It is a parameter to be always defined and known from the begging of each simulation.

b) **Reference axis**

The origin of the reference axis is defined at the center of mass of the structure where the hydrophones are fixed, which in this case is the AUV.

c) **Injected error**

In order to make the study more realistic, an $e_i$ error is added to the time differences of arrival, $\Delta t_{ij}$. These errors are mutually independent and follow a Gaussian distribution with zero mean and a configurable variance of $\sigma^2$, i.e., $e_i \sim \mathcal{N}(0, \sigma^2)$.

For the simulations performed in this project, a deviation of 5°, or a window of $[-2.5°, 2.5°]$, in phase difference estimation of incoming singals was considered to be reasonable for an underwater navigation scenario. Therefore, since the specified period of the signal is $T = \frac{1}{24400}$ and one period corresponds to a 360° phase shift, then the 5° will be equivalent to $\frac{5°}{360°} * T$ which is approximately a deviation of $0.5\mu s$. Hence the considered standard deviation $\sigma$ of the error $e_i$ in the computed time differences of arrival is equal to $0.5\mu s$.

Overall, the considered total time of arrival is equal to the measured time between the transmitter and the receiver through correlation, added by the computed time difference of arrival for a specific pair of hydrophones and the injected error $e_i$ in seconds.

d) **Acoustic source position**

The considered positions for the acoustic source, $s$, are originally defined in spherical coordinates, $s_{sph}$. Thus the norm, $n$, corresponds to the source's range in meters, whereas the azimuth, $\phi$, and elevation, $\theta$, define the angle of arrival of the received signal in degrees. Additionally, when these positions are mentioned in Cartesian coordinates throughout the document, they will be referenced as $s_{cart}$.

Recalling the definition of spherical coordinates, it is known that for elevations of -90° or 90°, the azimuth angle is meaningless and should not be considered. Since this system is affected by a Gaussian error, then the estimated azimuth angle is expected to return large errors not only for the absolute mentioned elevation values but for a considerable interval around it, dependent on the injected deviation. For that reason, the elevation values are limited to an interval between -80° and 80° so that the evaluated metrics present a result that is not so reflective of the errors originated from this phenomenon.

The positions to be estimated are contained in a matrix with a number of columns equal to the number of positions and three rows consisting of its spherical coordinates. The matrix is arranged so that for each defined norm, the elevation component covers the interval [-80° to 80°] in steps of one and, for each elevation value, the azimuth component covers the interval [-180°, 180°] in steps of one, forming partial spheres around the reference axis' origin.

e) **Propagation speed**

In all performed simulations, the considered speed of sound is $1500\,m/s$, which corresponds to the underwater propagation velocity of waves in typical conditions.

Having the conditions enumerated, the logic of the algorithm occurs as follows. For every defined position of the acoustic source, $s$, a function that consists on the estimator is called, receiving as input the $s$, the positions of the hydrophone configuration, $r_i$, and an injected error in the . It then returns the estimated position of the source in Cartesian coordinates, $[x, y, z]$, and in spherical coordinates, $[n, \phi, \theta]$. As the position $s$ in Cartesian corresponds to the real value that is intended to be estimated, we can also obtain the real spherical coordinates by directly converting $s$ using the Cartesian to spherical relations in 4.36.

$$\begin{cases} n = \sqrt{x^2 + y^2 + z^2} \\ \phi = arctan\frac{y}{x} \\ \theta = arctan\frac{\sqrt{x^2+y^2}}{z} \end{cases} \tag{4.36}$$

Consequently all conditions are met to analyze the achieved error in each coordinate by comparing the real position to the estimated values as 4.37, where the tested coordinates are $x, y, z, n, \phi$ and $\theta$.

$$error_{coordinate} = |estimated_{coordinate} - real_{coordinate}| \tag{4.37}$$

The metrics used to evaluate the quality of the estimator were :

- **Mean squared error** (MSE): Incorporates both the variance and the bias of the estimator, indicating its overall quality
- **Standard deviation of the error** ($\sigma$) : Indicates how disperse are the estimates from the expected value
- **Minimum error** ($min(e_i)$) : Indicates the minimum error that is obtained by the estimator, thus the best absolute precision achieved

#### 4.2.5.1 Functional analyzes of Monte Carlo TDoA estimator

Since this Monte Carlo algorithm was developed for this specific application, then it is possible to test diverse parameters of the system in order to characterize it. Therefore, a series of detailed simulations were performed using the TDoA estimator to understand the behavior, capabilities and the impact of some design decisions on the overall accuracy.

To illustrate a scenario where this estimator is applicable, we can consider that a vehicle is moving towards an acoustic signal transmitter whose position is unknown. Imagining that the target is at a considerable distance, then the main focus is to achieve an optimal bearing estimation which provides a more direct path and saves resources. The range estimation serves as secondary measurement that indicates how near the vehicle is from the destination, so that it is possible to make control decisions such as moderate the navigation speed in the proximity of the target. For the reasons outlined, the study that follows presents a more thorough analysis of the azimuth and elevation errors.

For the data visualization, two essential types of representation were developed :

- A 2D static representation of the error per position $s$. The errors to be tested are coordinates $x, y, z$, norm, azimuth angle or elevation angle.

- A 3D map of the obtained error. The x-axis holds the azimuth angle in degrees, the y-axis holds the elevation angle in degrees and the z-axis represents the measurement of a chosen parametric error. This allows to visualize, for a chosen configuration, how the estimation quality evolves in space.

For the first simulation, configuration A is tested for the acoustic source positions $s$ previously described, in a total of 58121, with a norm equal to 10 meters. Upon simulation, it is possible to observe that the geometric symmetrical nature of the configuration leads to estimation error patterns. Accordingly, it is possible to characterize the tendency of the azimuth and elevation errors according to the range of spherical coordinates angles. Table 4.3 summarizes these relations, where the arrows indicates if the error tendency is ascendant $\nearrow$ or descendant $\searrow$.

| | Range | Azimuth error | Elevation error |
|---|---|---|---|
| Azimuth angle | $-180°$ to $-90°$ | $\nearrow$ | $\searrow$ |
| | $-90°$ to $0°$ | $\searrow$ | $\nearrow$ |
| | $0°$ to $90°$ | $\nearrow$ | $\searrow$ |
| | $90°$ to $180°$ | $\searrow$ | $\nearrow$ |
| Elevation angle | $-90°$ to $0°$ | exponential $\searrow$ | $\searrow$ |
| | $0°$ to $90°$ | exponential $\nearrow$ | $\nearrow$ |

Table 4.3: Azimuth and elevation errors slope tendency for configuration A

By analyzing the collected information, it is possible to deduce that since the configuration's geometric center is located along the x-axis, then for elevation angles increasingly closer to $0°$ the errors have a tendency to decrease. Moreover, adding the fact that the depth of the baseline along the x-axis is shorter then the remaining, it results in a better azimuth estimation and a worst elevation estimation near an azimuth angle of $180°$ or $0°$. Overall, the maximum achieved errors are: for azimuth error $\approx 7.55°$, for elevation error $\approx 1.41°$ and for norm error $\approx 0.25$m, which corresponds to 2.5% of error in norm estimation.

For the same conditions, the maximum resulting $x, y$ and $z$ errors are: for $x \approx 0.28m$, for $y \approx 0.037m$ and for $z \approx 0.038m$. It should be pointed out that there is a higher error in the $x$ coordinate, which corresponds to the direction of the shorter baseline that consequently originates a greater uncertainty.

From this experiment, it was possible to collect the standard deviation and the minimum estimation error achieved for the azimuth and elevation angles, which are present further ahead in **??**. It should be noted that the chosen configuration A for the former analysis is by no means an optimal solution for the estimation. This particular layout was selected because it emphasizes several system responses to distinct configuration characteristics, allowing to understand how should them be adapt to achieve better results.

In order to further analyze the influence of the hydrophones placement in the estimation and which design choices lead to better estimations, two more scenarios are considered to test different aspects:

- **Influence of range in estimation**: In order to compare the range influence on the estimation, a second simulation intends to test the same configuration for a norm of 100 meters. The azimuth and elevation estimations do not demonstrate any visible changes in terms of range and the norm error increases for a maximum of $2.65m$, which still corresponds to approximately 2.6% error from the original norm. However, the $x, y$ and $z$ estimation demonstrate an error increase of about 10 times, since a small deviation in angle can correspond to a large difference in Cartesian coordinates. Nonetheless, for increasing ranges these errors stay proportional, so the error percentage is similar in any range. This phenomenon is illustrated in 4.9, where the error in $x$ is represented for all the tested positions that form spheres with norms equal to $10m$, $100m$ and $1000m$. As it is observed, the errors increase proportionally with the norm.

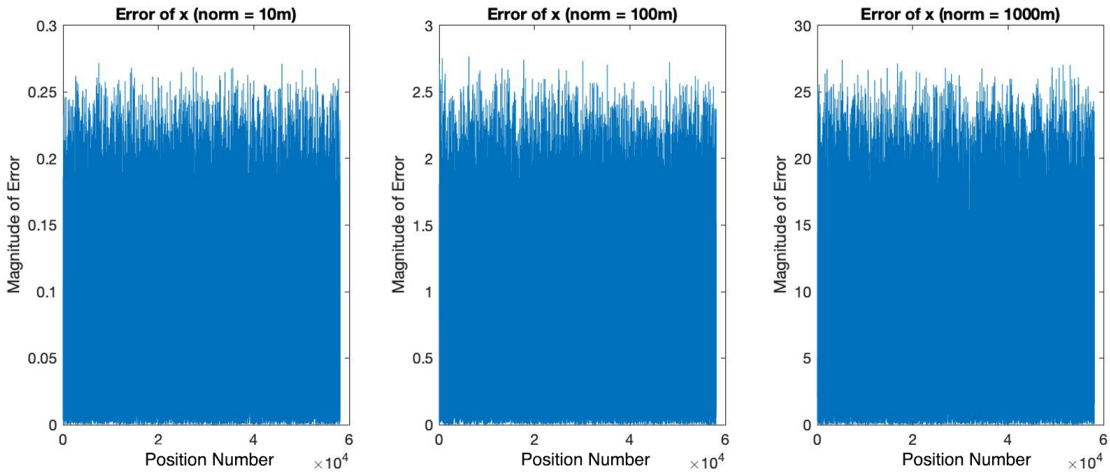


Figure 4.9: Evolution of error in Cartesian coordinates for increasing norm

- **Increasing the shorter baseline**: Since there are some issues that can be observed due to the short baseline along the x-axis, a third simulation serves to understand the influence of increasing this baseline in the estimation. Therefore, the baseline is increased by employing configuration B. After the simulation, the errors decreased visibly, which are indicated in 4.4.

After analyzing a specific configuration which demonstrate various limitation due to its arrangement design, it is desirable to compare it with different hydrophone placements. Therefore, table 4.4 contain the achieved results of MSE, standard deviation and minimum error for azimuth and elevation estimation in degrees, using norms equal to 10 and 1000 $m$ for configurations A, B and C. Configuration A represents an almost flat structure, configuration B is

a variation of A with an increased depth and configuration C resembles an AUV shape. By inspection it is possible to conclude that configuration B returns the lowest standard deviation and MSE, as it is also the one with the larger baselines between sensors.

| | | | Azimuth | | Elevation | |
|---|---|---|---|---|---|---|
| Configuration | Norm | MSE | Standard Dev | Minimum | Standard Dev | Minimum |
| A | 1 | 0.558 | 0.621 | $2.631\times10^{-5}$ | 0.192 | $3.262\times10^{-7}$ |
| | 1000 | 0.542 | 0.599 | $8.378\times10^{-6}$ | 0.185 | $5.059\times10^{-6}$ |
| B | 1 | 0.164 | 0.147 | $2.383\times10^{-6}$ | 0.052 | $1.387\times10^{-6}$ |
| | 1000 | 0.161 | 0.144 | $1.494\times10^{-6}$ | 0.050 | $4.910\times10^{-7}$ |
| C | 1 | 0.201 | 0.184 | $2.635\times10^{-6}$ | 0.061 | $5.772\times10^{-6}$ |
| | 1000 | 0.223 | 0.212 | $4.096\times10^{-6}$ | 0.066 | $4.394\times10^{-6}$ |

Table 4.4: Obtained errors for configurations A,B and C by TDoA estimator

Having explored the behavior of the estimator in specific conditions, there are still factors which were not discussed that may influence the system's performance or lead to an improvement. Therefore, four main ideas will be explored regarding the influence of the numeric quantization on the estimation accuracy, weather the absolute ToA is absolutely necessary for the position estimation, how is the estimates' dispersion for a specific position due to the injected error and the influence of increasing the baseline to the estimation accuracy.

**a) Influence of numeric quantization on accuracy** The first term to be analyzed is how much does the quantization of the calculations influence the obtained accuracy of the estimator. In order to analyze this, a simple adaptation was made to the numeric precision of the TDoA values that are input of the system. Instead of using the MATLAB precision of fifteen decimal places, the value was truncated to a specified number of decimal places, $\kappa$. Since the time differences of arrival have magnitudes around microseconds, then initially they are multiplied by $10^6$ to avoid missing information. Then the relation 4.38 is applied resulting in a truncated value with $\kappa$ decimal places. Finally after the truncation, the value is converted again to seconds to be used in the algorithm.

$$truncated = \frac{round(*2^{\kappa})}{2^{\kappa}}; \tag{4.38}$$

To evaluate the influence of the truncation in the estimation, configuration C is used to test a norm equal to 10. The original measurements are already represented previously. For a $\kappa$ of one decimal place, the azimuth standard deviation is 0.261 degrees, the elevation standard deviation is 0.087 degrees, the norm standard deviation is $0.014m$ and the MSE is 0.272. Overall, the estimation errors increase but, in practical terms, the truncation causes near to any difference in the estimation.

Since one decimal place does not bring too much discrepancy, the limit case is tested where zero decimal places are considered. In this case, the azimuth standard deviation is 0.416°, the elevation standard deviation is 0.136°, the norm standard deviation is 0.0209$m$ and the MSE is 0.439. As observed, the estimations are more influenced, however they still do not compromise the reliability of the estimation.

**b) Impact of ToA measurement on position estimation** As previously mentioned, the estimator uses the approximation explained in 4.2.1.4 which allows all hydrophones to use the same reference ToA added by a TDoA, representing the full distance between each hydrophone and the transmitter. However, for long range positions the ToA is consequently much larger in relation to the time differences of arrival. So, the hypothesis is that for these cases the ToA is irrelevant for the calculations and the TDoAs can be used alone to estimate the angle of arrival.

In order to simulate this, the calculated reference time is substituted by $\frac{10^4 m}{1500 m/s}$, which corresponds to a distance of 10$km$. The results demonstrated no visible change in the error of the estimate. However, for distances bellow 100$m$ the impact of this approximation starts to be noticed. Therefore, it is considered that the hypothesis is valid.

**c) Analysis of estimates' dispersion due to injected error** So far, the errors that have been analyzed correspond to a random executed simulation, which is influenced by an injected error equivalent to 5°. If the exact same experiment is executed several times, although the returned values have the same magnitude, they are only similar and rarely the same. Therefore, if each estimation is repeated a defined number of times, then the estimates can be analyzed so that it is possible to extract a single mean value which translates the estimation error.

In order to simulate this mechanism, an adaption was introduced in the previous algorithm. For each transmitter position $s$, the estimation is reiterated a specified number of times and, in each round, the azimuth and elevation errors are accumulated. After all samples are collected for a specific position, the azimuth/elevation deviation is calculated as the standard deviation of the accumulated azimuth/elevation errors and the azimuth/elevation errors are considered to be the mean of the accumulated azimuth/elevation errors. After the measurements are executed for every position in space, it is computed the overall azimuth and elevation errors and deviations which characterize the specific chosen configuration, as well as the final MSE.

For exemplification purposes, configuration C was tested 100 consecutive times with no reiterations for each position, 4.10, and with 100 accumulated samples, 4.11 in order to verify the dispersion of the obtained results. As it is observed, when the error is averaged with accumulated samples, there is a smaller discrepancy among the results.

This approach allows to achieve more coherent results and to characterize the configurations in a more methodical manner.

**d) Influence of increasing the configuration baseline** Until this point, there are several mentions to the baseline of the used configuration and its numeric impact on the estimation

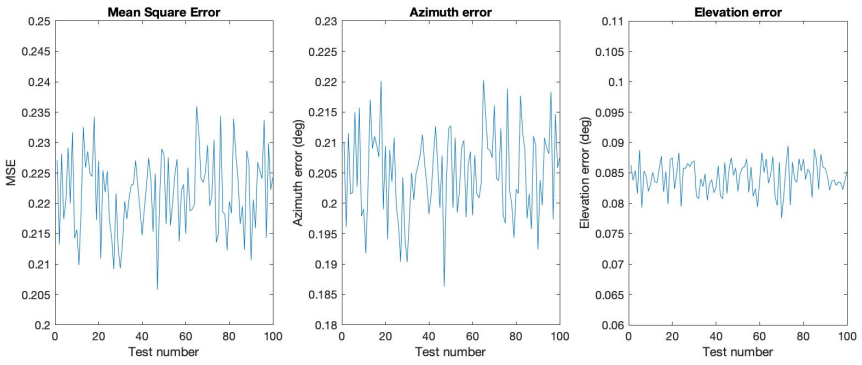


Figure 4.10: Obtained error for a single configuration with no accumulated samples

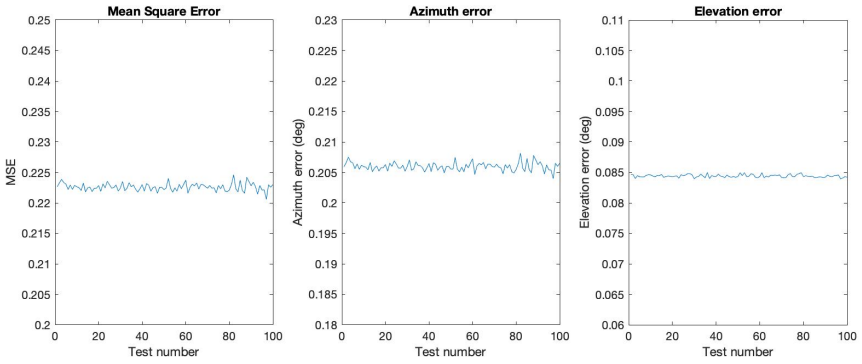


Figure 4.11: Obtained error for a single configuration with 100 accumulated samples

performance. However, there are no conclusions about the optimal baseline that should be used. The goal of this test is to delineate the influence of increasing the hydrophones' baseline in the obtained error.

In order to execute this test, configuration C is used as well as the method previously explained that reiterates each estimation a defined number of times to achieve average dispersion values. To create an increasing baseline along the tests, in each iteration the $x$ coordinate of $r_{C1}$ increases $0.01m$ in a total of 200 times, which makes up a displacement range between 0.1 and $2m$. Each position generates 100 accumulated samples that result in a single measurement per configuration.

Plot 4.12 represents the collected errors for each of the described configurations, whose baseline is progressively increasing in a constant pace. As illustrated, the obtained errors decrease visibly in the first 100 tests, corresponding to a $r_{C1}$ position between 0.1 and $1m$, becoming considerably constant for further distances.

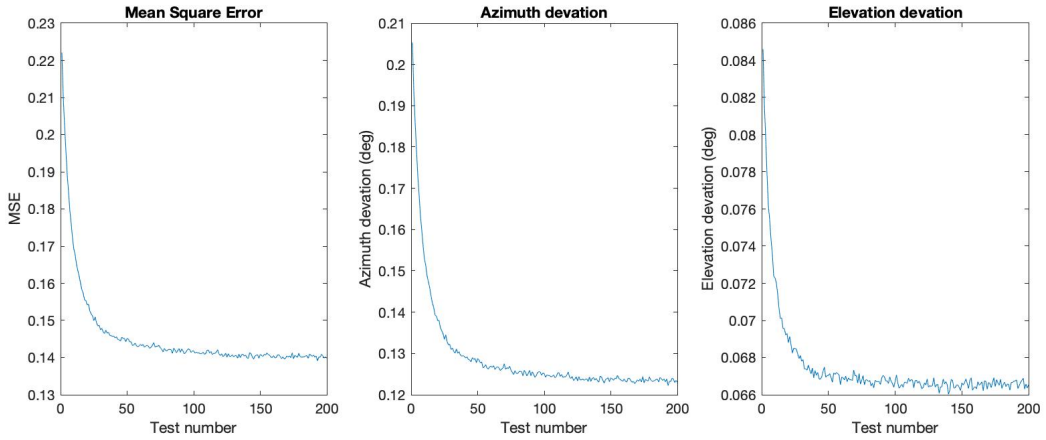


Figure 4.12: Error evolution with increasing baseline for $r_{C1}$

Additionally, the same experiment was done on hydrophone $r_{C2}$ of the same structure, since its position on the configuration gets a different exposure than $r_{C1}$ and a different outcome is expected. Having considered the same conditions as explained for the previous simulation, figure 4.13 illustrates the obtained results. It can be observed that the displacement of this specific hydrophone only causes an estimation improvement in the elevation deviation, it does not affect the estimation of the azimuth deviation and slightly increases the azimuth deviation. Therefore, an estimation improvement may not be achieved by distancing a random hydrophone, a study should be conducted for each particular configuration to determine which displacements lead to an enhancement.

In conclusion, it is proved that increasing the baseline of a configuration in specific cases may result in a decrement of the overall estimation error. However, this only occurs for a maximum distance after which the error becomes constant.

**e) Conclusions on TDoA based estimator** The present chapter focused on detailing the developed estimator, including the involved mechanisms and algorithm, a behavioral analysis and

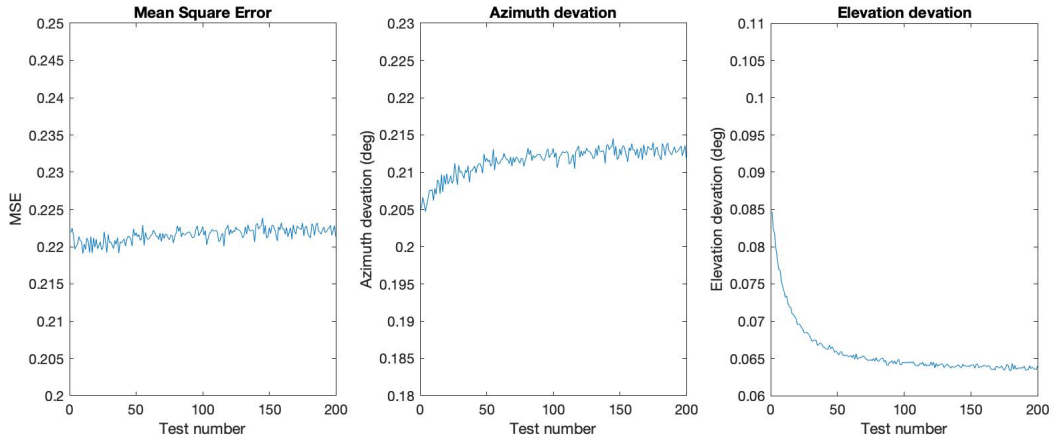


Figure 4.13: Error evolution with increasing baseline for $r_{C2}$

characterization based on simulated results. Therefore, by way of summary, some main conclusions can be taken:

- The azimuth and elevation errors do not vary with the range of the transmitter's position, in contrast to errors in Cartesian coordinates which increase proportionally with the range;
- The ToA measurement is not essential for long range distances. So, in those cases there is no need for synchronization since a random large ToA can be used instead;
- A lower numeric precision in the calculations affects the obtained results, however since in the explored situations the errors are inherently small, the error increase does not have an impact on the system from a practical point of view;
- Increasing the baseline of a hydrophone configuration can result in a better estimation, until reaching a certain distance after which the error becomes constant. Therefore, when choosing an hydrophone layout which can be limited to the dimensions of a physical structure, it does not have to be sought the maximum baseline possible but the length that leads to the error becoming constant;
- Applying a reiteration process to create averaged errors for each configuration, creates results which are more consistent thus more capable of characterizing a specific process. Additionally, the random nature of the Monte Carlo approach is attenuated, resulting in more coherent results.
- The hydrophone configuration is a main factor on the estimation performance for any position in space. Although the characteristics that a configuration should meet to be optimal are still not clear, some aspects can be pointed out:
  - It is mandatory to ensure a sensor layout which covers three dimensions, so it is possible to estimate coordinates in 3D;

– The positions of the sensors must be linearly independent to allow the application of the least squares method;

– It is fundamental to have an adequate baseline which can be determined with the tool previously explained;

– Bearing in mind that the configuration may be employed in real scenarios, it is useful to create schematics which require achievable distances between hydrophones and respect logical shapes to install in vehicles such as AUVs.

#### 4.2.5.2 Functional analyzes of Monte Carlo plane wavefront estimator

In order to understand the basic behavior of the plane wavefront estimator, it was tested at first for the estimation of a single position. An injected error is considered according to the initial defined circumstances in 4.2.5, which is added to the calculated ToA to each sensor. So, a series of 1000 iterations are performed to the estimation of position $s_{cart}(0,100,0)$ using configuration A and the obtained estimations are represented in 4.14.

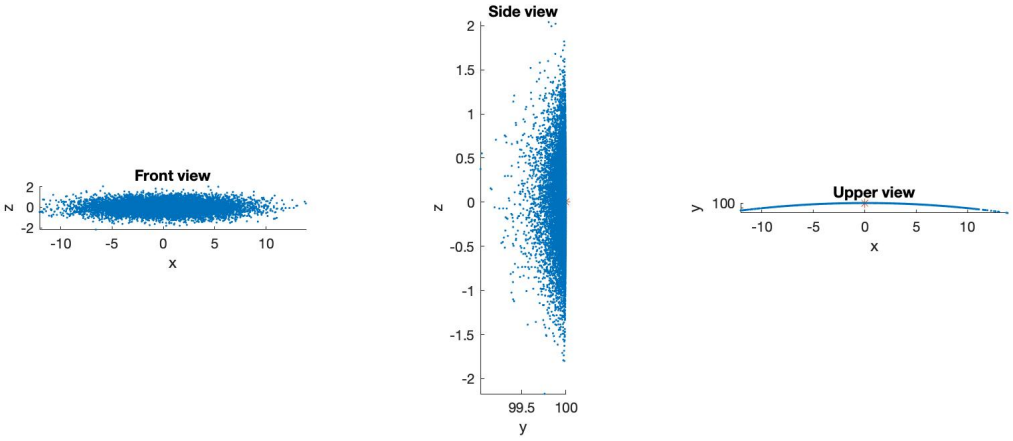


Figure 4.14: Estimation of position $s_{cart}(0,100,0)$ using the plane wavefront estimator with configuration A

As can be observed, the upper view reveals that the estimates are placed along a sphere surface, which corresponds to the expected result since the norm is calculated as the average ToA while the direction estimation is influenced by the error that affects the TDoAs. Additionally, the front view, which represents the view from the origin to the estimated position in the y-axis, reveals a narrow estimate cloud with larger error in azimuth. However, by inspection it is possible to conclude that this relation varies according to the position that is being estimated and is not a constant proportion.

After analyzing this specific case, a second simulation intends to achieve a more comprehensive study on the performance sensor configurations. Therefore, using a specific configuration, all $s$ positions that form a sphere of defined norm were estimated a total of 1000 times, in order for the errors to be averaged, and the relevant data is retrieved, namely the

standard deviation and minimum error of both azimuth and elevation estimations. The results are summarized in table 4.5, where configurations A, B and C are tested for norms equal to 10 and 1000 meters.

| | | | Azimuth | | Elevation | |
|---|---|---|---|---|---|---|
| Configuration | Norm | MSE | Standard Dev | Minimum | Standard Dev | Minimum |
| A | 1 | 0.346 | 0.151 | 0.234 | 0.143 | 0.191 |
| | 1000 | 0.331 | 0.178 | 0.233 | 0.176 | 0.230 |
| B | 1 | 0.322 | 0.160 | 0.224 | 0.159 | 0.212 |
| | 1000 | 0.332 | 0.173 | 0.234 | 0.170 | 0.222 |
| C | 1 | 0.410 | 0.241 | 0.322 | 0.167 | 0.235 |
| | 1000 | 0.410 | 0.242 | 0.322 | 0.170 | 0.231 |

Table 4.5: Obtained errors for configurations A,B and C using a plane wavefront estimator

table interpretation

#### 4.2.5.3 Functional analyzes of Fisher Information Matrix

In order to demonstrate the functionality of the described method, a first simulation was conducted in which a chosen configuration is tested for various positions $s$, returning the uncertainty sphere radius, in meters, that is obtained for each position. Similarly to what was considered before in 4.2.5, for each defined norm, the elevation component covers the interval [-90° to 90°] in steps of one and, for each elevation value, the azimuth component covers the interval [-180°, 180°] in steps of one, forming partial spheres around the reference axis' origin. The simulation was conducted using configuration C previously defined.

When estimating positions correspondent to a sphere of norm equal to $100m$, the obtained results are illustrated in figure 4.15, which show the uncertainty sphere radius for each of the $s$ positions, with respect to azimuth and elevation angles. The first plot represents the 3D map of each radius in relation to both angles, the second plot is a 2D view of the uncertainty with respect to the azimuth angle in degrees and the third plot is the 2D view of the uncertainty with respect to elevation angle in degrees.

In this specific case, it is noticeable that this configuration is capable of better estimations for low elevation angles and has an ascendant error for increasing elevation angles. Additionally, the uncertainty has a tendency to increase for azimuth angles around $-90°$ and $90°$. Overall, for a norm equal to $100m$, the standard deviation of all estimations is $0.0029m$ and the best estimation occurred for position $s_{sph}(100,-180,3)$ in spherical coordinates, with an uncertainty radius of $0.0532m$.

This tool also makes it possible to analyze the specific uncertainty ellipsoid of a position estimate, i.e. each of the eigenvectors of the FIM, for a specific configuration. Then, resorting tho the same configuration C, it is observed that for any estimated position, the eigenvector parallel to

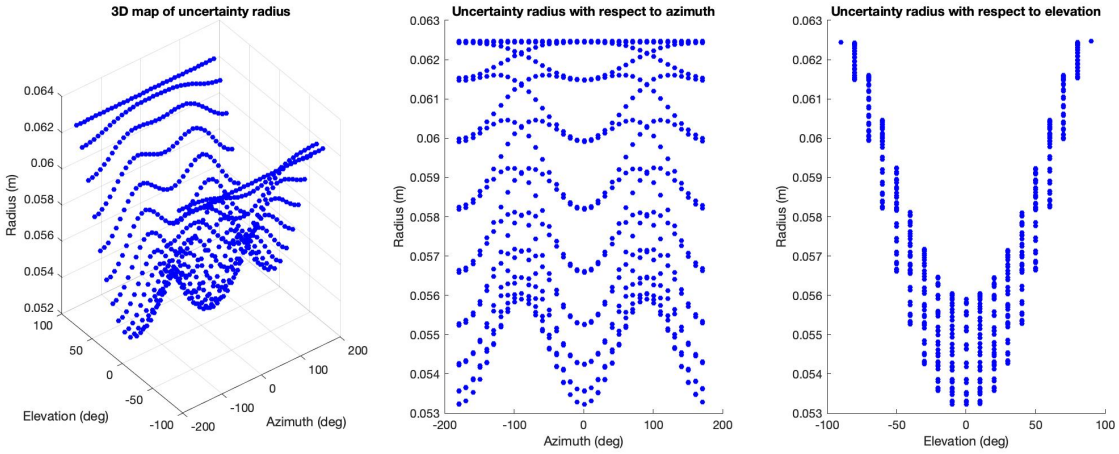


Figure 4.15: Uncertainty radius obtained by configuration C for all sphere positions

the direction of the angle of arrival always demonstrate the smaller uncertainty. This corresponds to what is expected since the injected error affects the TDoA which has a direct influence on the angle of arrival while the ToA is estimated using absolute distances. Additionally, for any estimated position it is also observed that, if it is considered a vector connecting the origin to the transmitter position, this vector forms angles with the eigenvectors that have an approximated uniform pattern: there is always two angles which are close to 90°, correspondent to errors in azimuth and elevation angles, and one angle that is close to 0°, correspondent to the norm error.

Figure 4.16 illustrates this concept for a estimation of position $s_{cart}(10,0,0)$. As indicated the first plot represents the side view, plane zx, and the third plot illustrates the view from above, plane yx, which illustrate to the norm error, the second plot represents the USBL front view, plane zy, which corresponds to the error in azimuth and elevation angle.

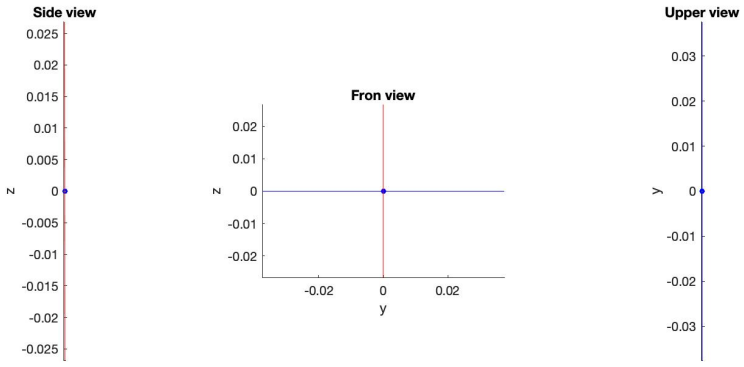


Figure 4.16: Eigenvectors obtained for configuration C when estimation position $s_{cart}(10,0,0)$

Finally, similarly to the previous methods a final simulation was ran on configurations A, B and C in order to evaluate their performance on the estimation of several defined positions

along a sphere with norms of 10 and 1000 meters. Since the Crámer-Rao lower bound does not contemplate the azimuth and elevation errors as an optimality criteria, then other metrics are used in this case. Table 4.6 contains the obtained data, including the criteria with the following meaning:

- **Determinant of the inverse of the FIM**: reflects the uncertainty sphere radius
  - Minimum: corresponds to the smallest uncertainty sphere radius achieved by the configuration. Represents the most accurate estimate among all estimated positions, thus an optimistic case;
  - Maximum: corresponds to the biggest uncertainty sphere radius achieved by the configuration. Represents the estimate with lower accuracy among all estimated positions, thus a pessimistic case;
  - Standard deviation: corresponds to the standard deviation of the obtained determinants of the inverse of the FIM for all estimated positions. Reflects the variance of the estimates.
- **Maximum Eigenvalue of the inverse of the FIM**: considering the uncertainty ellipsoid, which presents three uncertainty axis with distinct magnitudes, this parameter reflects the maximum uncertainty that is achieved for each position
  - Minimum: considering that each configuration obtains a maximum eigenvalue for each estimated position, this parameters corresponds to the position whose largest uncertainty is minimized.
- **Trace of the inverse of the FIM**: reflects the sum of the magnitudes of the uncertainty axis for each estimated position
  - Minimum: corresponds to the minimum of the uncertainty average variance, thus the positions that reveals a the lowest summed uncertainty magnitudes

| | | Determinant | | | Max Eigenvalue | Trace |
|---|---|---|---|---|---|---|
| Configuration | Norm | Min | Max | Std | Min | Min |
| A | 1 | $2.2\times10^{-3}$ | $4.2\times10^{-3}$ | $6.65\times10^{-4}$ | $5.3\times10^{-3}$ | $5.60\times10^{-5}$ |
| | 1000 | 0.220 | 0.421 | 0.067 | 5.310 | 56.325 |
| B | 1 | $2.1\times10^{-3}$ | $2.5\times10^{-3}$ | $8.78\times10^{-5}$ | $5.3\times10^{-3}$ | $5.17\times10^{-5}$ |
| | 1000 | 0.2193 | 0.2462 | 0.008 | 5.306 | 56.283 |
| C | 1 | $2.5\times10^{-3}$ | $3.0\times10^{-3}$ | $1.39\times10^{-4}$ | $7.1\times10^{-3}$ | $8.42\times10^{-5}$ |
| | 1000 | 0.247 | 0.290 | 0.014 | 7.410 | 84.882 |

Table 4.6: Obtained errors for configurations A,B and C by Crámer-Rao lower bound

conclude

### 4.2.6 Final remarks

This section focuses on three selected methodologies that are capable of evaluating sensor configurations' performance based on multiple criteria.

Firstly, a Monte Carlo estimator based on TDoA is presented, which is expected to demonstrate better results for short range estimation since the very precise computed TDoAs become more relevant in the calculation. However, due to the system's non linearity, the results may be different than the expected and it should be used taking that detail into account.

Secondly, a Monte Carlo estimator based on a plane wavefront is considered, which is expected to have better performance for long range estimation, since the assumed approximation affects the system less for long distances and it is derives linear results. However, in short range estimation this method is expected to express larger estimate error, due to the fact that the angle of arrival to each hydrophone is considerably different, so the plane wavefront should not be considered.

Lastly, the Crámer-Rao lower bound method is applied, which makes use of the Fisher Information Matrix. As the FIM reflects the quantity of information that a configuration is capable of acquiring in relation to a specific position, then it can be directly related to the accuracy of the estimation. This method assumes the use of any unbiased and efficient estimator, which makes it a more generic tool. Consequently, it is widely used in literature for sensor configuration's performance analysis and it is expected that it shows the most reliable results for this application.

# Chapter 5

# Adaptive configuration selection method

Having studied the estimator's behavior for several different configurations and conditions, there is still uncertainty about the best performance it can achieve. In the considered system, the hydrophone configuration has a decisive role on the achieved precision, as demonstrated. Therefore, a way to optimize the system's estimation would be to choose, for each position of the acoustic source, the configuration that returns the best estimation and thus the one that should be employed.

In a field scenario where a vehicle is searching for an acoustic transmitter, as it is navigating and readjusting its trajectory, the relative direction that is being estimated in real time is changing. Therefore, the system's performance can vary and arises the necessity of having different angles of vision from the hydrophones to the target. To resolve this issue, the proposed method assumes that the used USBL system integrates more than four hydrophones placed in known positions. This way, it is possible to dynamically reconfigure which four hydrophones are used at a time leading to an estimation that is optimal for the available sensors.

Another possibility is to determine through the same techniques which configuration of four hydrophones, tested in various positions along the vehicle, is the overall best for short and long range estimation. This can lead to a moderate compromise of the estimate accuracy, however decreases the number sensors that are employed and therefore the cost of the system.

This chapter is dedicated to explaining the methodological approach, the main findings and conclusions that were driven from the formulated optimal reconfiguration method. Firstly, the developed Monte Carlo method is explained, including the theoretical details as well as the developed algorithm. Thereafter, its functional demonstration through simulation is presented, followed by a brief comparison with the results obtained by the Crámer-Rao bound method previously implemented. Lastly, the implementation of the optimal solution based on range is presented and a practical comparison is established with the alternative FIM mechanism.

## 5.1 Monte Carlo Approach

The developed algorithm serves as a tool to determine which is the best available hydrophone configuration for a certain target position. This approach uses a Monte Carlo method which is useful to solve problems that are deterministic in nature through repetition and application of random parameters. Additionally, it makes use of the developed estimator, which is comprehensively explained in 4.2.2, to estimate the target position for each sensor configuration.

For this experiment, it is considered a total of nine hydrophones, whose positions are contained in $matrix_{r_i}$, defined by table 5.1. Each column expresses the coordinates of each hydrophone, $r_i$, where the value of $x_i$ is in the first row, the value of $y_i$ in the second row and the value of $z_i$ in the third row. Additionally, it is assumed $q = 0.1$, $w = 0.1$ and $e = \frac{\sqrt{2}}{2} * w$.

| | r1 | r2 | r3 | r4 | r5 | r6 | r7 | r8 | r9 |
|---|---|---|---|---|---|---|---|---|---|
| x | q | 0 | 0 | 0 | 0 | 0 | 0 | 0 | 0 |
| y | 0 | 0 | 0 | w | -w | e | e | -e | -e |
| z | 0 | w | -w | 0 | 0 | e | -e | e | -e |

Table 5.1: Position coordinates for the implementation using 9 hydrophones

These positions are arranged so that they can mimic a possible deployment in an AUV, as represented in figure 5.1, where hydrophone $r_1$ is placed in front of the vehicle and hydrophones $r_2$ to $r_9$ form a circle with a $10cm$ radius around the vehicle.

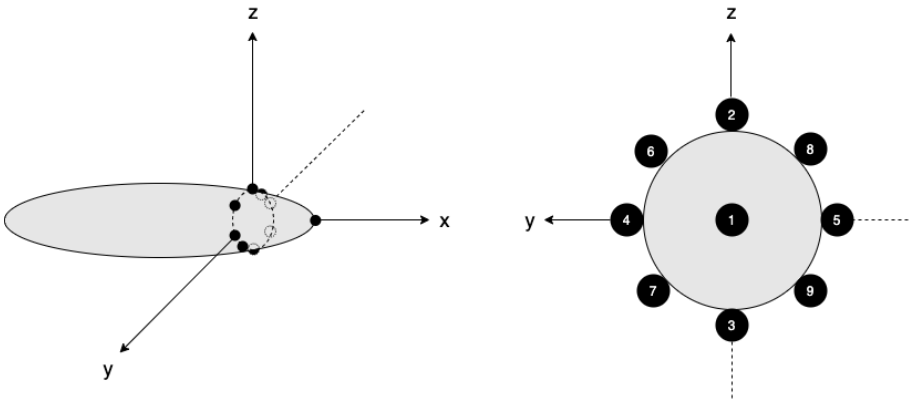


Figure 5.1: Hydrophone positions for the implementation using 9 hydrophones

Since the used configuration has to be three dimensional, it is defined that hydrophone $r_1$ always integrates the configuration as it is the only one that covers a third dimension. Accordingly, the number of possibilities is combinations of three out of eight, $C(8,3)$, making up a total of 56 combinations. Each of these configurations are associated with a number from 1 to 56 and the hydrophones that integrate each of them are outlined in table A.1 for consultation when necessary.

Having the system presented, the algorithm will be explained next. For the sake of clarity, the algorithm was outlined in pseudo code and separated into two main parts, where 1 is integrated in 2.

**Algorithm 1** Determines the average azimuth errors, elevation errors and MSE for a set of hydrophone configurations

1: **for** `all k configurations` **do**
2: **for** `all i estimation repetition` **do**
3: $estimator(s, config(k), error)$ {returns estimate in Cartesian and spherical coordinates}
4: `accum_estimate(i) ← result of the estimator in each repetition`
5: `accum_error_azimuth(i) ← azimuth error in each repetition`
6: `accum_error_elevation(i) ← elevation error in each repetition`
7: **end for**
8: $mean\_estimate \leftarrow \frac{accum\_estimate}{accum\_samples}$
9:
10: $deviation\_azimuth(config) = std(accum\_error\_azimuth)$;
11: $deviation\_elevation(config) = std(accum\_error\_elevation)$;
12: $error\_azimuth(config) = mean(accum\_error\_azimuth)$;
13: $error\_elevation(config) = mean(accum\_error\_elevation)$;
14:
15: $mse(config) = \sqrt{error\_azimuth(config)^2 + error\_elevation(config)^2}$;
16: **end for**

Algorithm 1 is dedicated to computing the average azimuth error, elevation error and MSE for each of the $k = 56$ hydrophone configuration, in order to understand which of them achieves the minimum deviations when estimating a specific position. In order to do so, for each possible hydrophone configuration, the chosen acoustic source position $s$ was estimated $i = 1000$ times (line 3), using the developed estimator. This includes an injected error to the TDoA that follows a Gaussian distribution with zero mean and a configurable variance of $\sigma^2$, i.e., $e_i \sim \mathcal{N}(0, \sigma^2)$. The result of this repetition would be an estimate cloud around the absolute $s$ position, which indicates the estimation variation achieved by a certain configuration for a specific position in space. At each stage of the repetition, the estimate is accumulated and the errors of azimuth and elevation are calculated, similarly to the process described in the accuracy analysis **??** of the estimator. Therefore, after computing all estimation repetitions, it is possible to extract four essential parameters that define the quality of the estimation for each configuration: a mean estimate (line 8); the azimuth and elevation standard deviations (lines 10 and 11); the azimuth and elevation estimation errors (lines 12 and 13); the MSE (line 15).

Finally, using the obtained parameters it is possible to determine three configurations that lead to the best estimation regarding MSE, azimuth deviation and elevation deviation. However, there are two main issues that this simple algorithm does not take into account:

1. For the considered system conditions, the error that is introduced is sufficient to originate different results every time a position $s$ is tested with the same injected error.

2. Assuming that the hydrophone system is deployed in an AUV, it is expected that every hydrophone has a blind spot, where the acoustic source can be located. Even though the

transmitted signals could still be received by these hydrophones, they would be distorted and could lead to misinformation so they should not be considered. Consequently the hydrophones that do not have line of sight to the transmitter should be disregarded as well.

In order to resolve both these problems, a second part of logic was developed, which is translated in pseudo code 2.

In order to turn this mechanism more robust and solve the first issue, it is considered that the experiment of algorithm 1 has to be reiterated a defined number of times to obtain coherent and conclusive answers. Having said this, algorithm 2 begins with a loop that reiterates $j = 10$ times the logic previously explained. Addressing the second issue, the *line_of_sight* function (line 7) is called, serving as filter to determine which hydrophones have line of sight to the estimated position. The mathematical definitions and conditions included in this function as well as the inputs and outputs are better clarified in the next subsection 5.1.1. Thereafter, all configurations that have full line of sight to the transmitter are extracted. Meanwhile, the azimuth deviations, elevation deviations and MSE are accumulated in each experiment reiteration (line 8 to 10) so that it is possible to obtain the definitive mean of these parameters for each configuration (line 12 to 14).

**Algorithm 2** Determines the overall best configuration for a specific position estimation considering:
- multiple full experiments (Algorithm 1);
- only hydrophones with line of sight to the target.

1: **for** `all j experiment reiterations` **do**
2: `**************************`
3: `*** INSERT ALGORITHM 1 ***`
4: `**************************`
5:
6: $line\_of\_sight(mean\_estimate, matrix_{r_i})$ {returns which hydrophones have line of sight to the target}
7:
8: $reit\_mse = reit\_mse + mse$
9: $reit\_dev\_azimuth = reit\_error\_azimuth + deviation\_azimuth$
10: $reit\_dev\_elevation = reit\_error\_elevation + deviation\_elevation$
11: **end for**
12: $mean\_MSE = reit\_mse \div j$
13: $mean\_dev\_azimuth = reit\_dev\_azimuth \div j$
14: $mean\_dev\_elevation = reit\_dev\_elevation \div j$
15:
16: `Extract the configurations that contain only hydrophones with line of sight`
17: `Form matrix with errors of only the configurations with full line of slight`
18:
19: $[best\_config\_for\_mse,\ overall\_min\_mse] = min(overall\_mse)$
20: $[best\_config\_for\_azimuth,\ overall\_min\_dev\_azimuth] = min(overall\_dev\_azimuth)$
21: $[best\_config\_for\_elevation,\ overall\_min\_dev\_elevation] = min(overall\_dev\_elevation)$

At this stage, it is possible to know already which are the configurations that are considered to achieve the minimum errors in each $j$ reiteration and how many times each of them are chosen. However, these are still not filtered, thus they can contain hydrophones that have not line of sight

to the acoustic source. Consequently, the next step is to extract only the configuration with full LOS and form three matrices with the azimuth deviations, elevation deviations and MSE of these configurations. Having the final parameters calculated and filtered, the overall best configurations for each of the chosen parameters are given by the minimum of the matrices that contain said parameter (line 19 to 21), i.e. for all configurations with full LOS:

- The minimum obtained MSE corresponds to the configuration that more precisely estimates the position $s$ in terms of MSE;
- The minimum obtained azimuth deviation corresponds to the configuration that more precisely estimates the position $s$ in terms of azimuth;
- The minimum obtained elevation deviation corresponds to the configuration that more precisely estimates the position $s$ in terms of elevation.

Additionally, it is possible to obtain the best configuration in terms of azimuth and elevation simultaneously, by computing the mean between the deviation of azimuth and elevation in each of the selected configurations. The minimum value obtained corresponds to the configuration which achieve the minimum the deviation in both parameters simultaneously.

### 5.1.1 Line of sight definition

As briefly explained before, when considering a set of hydrophones placed in the surface of an AUV, there will be blind regions for each of the hydrophones. Nonetheless, when an acoustic source is positioned in a blind region of an hydrophone, it still can receive a transmitted signal through reflections on path objects or reverberation in the AUV's surface. Since these signals would be distorted from the original, they could lead to misinformation after the processing if they were to be considered. For this reason, it is essential to exclusively consider configurations whose hydrophones have line of sight (LOS) to the transmitter.

In the present application, this feature is executed through function $line\_of\_sight$ of algorithm 2, which outputs a vector containing all the hydrophones that have line of sight to the inputted transmitter position, $mean\_estimate$, from the considered set $matrix_{r_i}$.

In order to define which hydrophones have LOS to a specific position in space, a region was defined for each hydrophone as its LOS region, $ls_i$. Thus, three simplifications were initially considered:

- The model for the vehicle is an approximation to a typical shape of an AUV using geometric shapes, as represented in 5.2, composed by a cylinder as the body with $2*w$ of diameter and a cone in the front with height equal to $q$;
- The regions for a $x \leq 0$ are defined as if the hydrophones were flat in the vehicle's surface, which leads to a simplified definition of the LOS region;

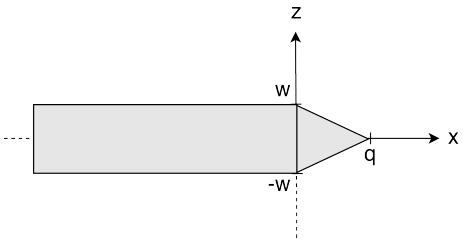


Figure 5.2: Model of AUV used to calculate the LOS region

- Since hydrophone $r_1$ is integrated in every configuration, there is no necessity of defining its LOS region.

Having these relations into account, the LOS regions are then defined separately for $x \leq 0$ and $x > 0$. When $x \leq 0$, the second simplification previously mentioned is applied so all $ls_i$ are defined as the region greater/less or equal than the tangential to the position of hydrophone $i$ in plane yz. These tangential equations are defined in 5.1 to 5.8.

$$ls_2 \leftarrow x \leq 0 \ \wedge \ z > r_{2_z} \tag{5.1}$$
$$ls_3 \leftarrow x \leq 0 \ \wedge \ z < r_{3_z} \tag{5.2}$$
$$ls_4 \leftarrow x \leq 0 \ \wedge \ y > r_{4_y} \tag{5.3}$$
$$ls_5 \leftarrow x \leq 0 \ \wedge \ y < r_{5_y} \tag{5.4}$$
$$ls_6 \leftarrow x \leq 0 \ \wedge \ z \geq -y + w\sqrt{2} \tag{5.5}$$
$$ls_7 \leftarrow x \leq 0 \ \wedge \ z \leq y - w\sqrt{2} \tag{5.6}$$
$$ls_8 \leftarrow x \leq 0 \ \wedge \ z \geq y + w\sqrt{2} \tag{5.7}$$
$$ls_9 \leftarrow x \leq 0 \ \wedge \ z \leq -y - w\sqrt{2} \tag{5.8}$$

By evaluating these equations, it is possible to infer that the LOS regions for $x \leq 0$ intersect each other, as illustrated in figure 5.3. The projection is correspondent to the yz plane with an inverted y-axis, in accordance with the previously presented model of the USBL system. Additionally, each colored line corresponds to the LOS region covered by the hydrophone with the same color. For instance, if a transmitter is located in $s_{cart}(-10,-10,-10)$, by analysis of the schematic it is observable that this position is covered by $ls_3$, $ls_5$ and $ls_9$, thus in line of sight of hydrophones 3,5 and 9.

Analogously, when $x > 0$, all $ls_i$ are defined as the region greater/less or equal than the tangential to the position of hydrophone $i$ in planes xz or xy, depending on the hydrophone's location. Dealing with the hydrophones positioned in the y and z-axis, $r_2$, $r_3$, $r_4$ and $r_5$, it is possible to directly formulate equations that help defining $ls_2$, $ls_3$, $ls_4$ and $ls_5$ since the tangent plane to these hydrophones is perpendicular to referential planes. However, when considering hydrophones $r_6$, $r_7$, $r_8$ and $r_9$, which are not positioned in any referential axis, the tangential plane which passes through the hydrophone and the front limit of the cone is not parallel to any of the

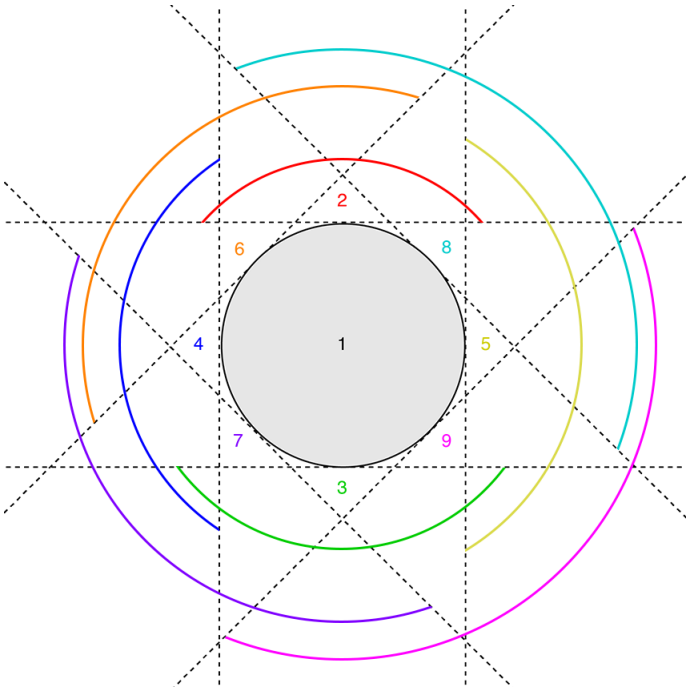


Figure 5.3: Line of sight regions in plane yz for x < 0

referential planes xy, xz or yz. Therefore, the equations that could define these planes require a rotation of the referential axis. In order to counter this issue, since the shape of the model projected in the yz plane is a circle , if hydrophones $r_6$, $r_7$, $r_8$ and $r_9$ are rotated a 45° angle around the x-axis, they can become coincident with the positions of $r_2$, $r_4$, $r_5$ and $r_3$ respectively. Additionally, when considering this rotation, the position of the transmitter would also be rotated the same angle to maintain their relative positions. Overall, the used equations are defined by relations 5.9 to 5.12, where the regarded $x, y, z$ coordinates are the original transmitter position for $ls_2$, $ls_3$, $ls_4$, $ls_5$, and the rotated transmitter position for $ls_6$, $ls_7$, $ls_8$, $ls_9$.

$$ls_2,\ ls_6 \leftarrow x > 0 \ \wedge \ z \geq -\frac{w}{q}x + w \tag{5.9}$$

$$ls_3,\ ls_9 \leftarrow x > 0 \ \wedge \ z \leq \frac{w}{q}x - w \tag{5.10}$$

$$ls_4,\ ls_7 \leftarrow x > 0 \ \wedge \ y \geq -\frac{w}{q}x + w \tag{5.11}$$

$$ls_5,\ ls_8 \leftarrow x > 0 \ \wedge \ y \leq \frac{w}{q}x - w \tag{5.12}$$

After evaluating these equations and the limiting planes that they form, the projected regions of LOS for $r_2$, $r_3$, $r_4$ and $r_5$ are illustrated in 5.4, where their intersection is evident. The regions $ls_2$, $ls_3$, $ls_4$ and $ls_5$ are naturally similar to these, with an additional rotation of 45° around the x-axis.

In summary, it is possible to deduce that there is a larger quantity of different configurations

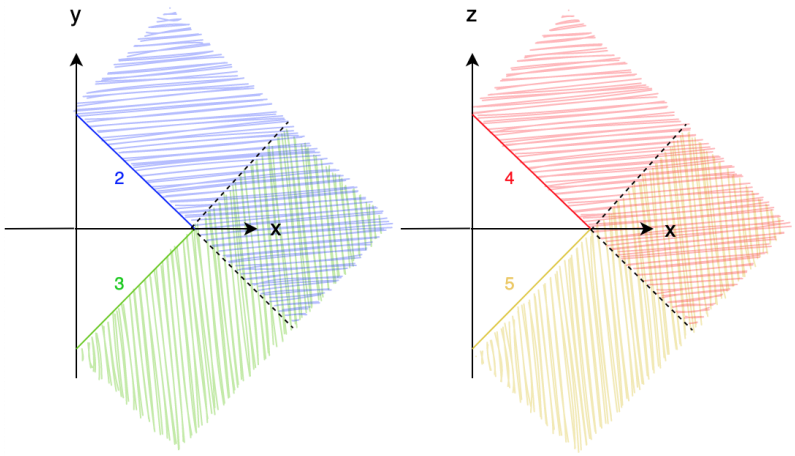


Figure 5.4: Line of sight regions in plane yx and zx for x $\geq$ 0

that cover the space for $x > 0$ than for $x \leq 0$ due to the model of the AUV and the considerations described in the course of this subsection. Therefore it is expected a better estimation for positions of the acoustic source with an azimuth angle between $-90°$ and $90°$.

## 5.2 ~~Comprehensive~~ study of geometric configurations performance

For the purpose of demonstrating the functionality of the implemented system, various acoustic source positions were tested and the results analyzed.

The first demonstration evaluates the achieved MSE, azimuth deviation and elevation deviation for $s_{cart}(10,10,10)$. After simulating, plot 5.5 demonstrate the results, where the obtained parametric errors are illustrated for each of the 56 formulated configurations. Additionally, the configurations which are marked with a red circle correspond to those whose hydrophones all have full line of sight to the transmitter and the green star indicates which is the configuration that achieves the lowest error. The results of this experiment are aggregated in table 5.2. For the present case, the hydrophones considered to have line of sight to the target are $r_2$, $r_4$, $r_6$, $r_7$ and $r_8$. The configuration with lowest MSE and azimuth deviation is number 8, composed by hydrophones $r_1$, $r_2$, $r_4$ and $r_6$, which are the directly closer to the target. The configuration that originates lowest elevation deviation is number 19, composed by $r_1$, $r_2$, $r_7$ and $r_8$, which maximizes the baseline of the sensors with line of sight.

Additionally, if the azimuth and elevation deviations are evaluated simultaneously, then the obtained plots can be overlaid to a clear comparison between results. Figure 5.6 represents this situation where, as the label indicates, the azimuth deviation in degrees is represented by the blue line, the pink line is the elevation deviation in degrees, the red and green circles represent the configurations with line of sight to the target and the green star indicates, once again, the configurations which achieve the minimum deviations in azimuth and elevation. Additionally, the cyan diamond reveals which of the configurations leads to the minimum mean between the

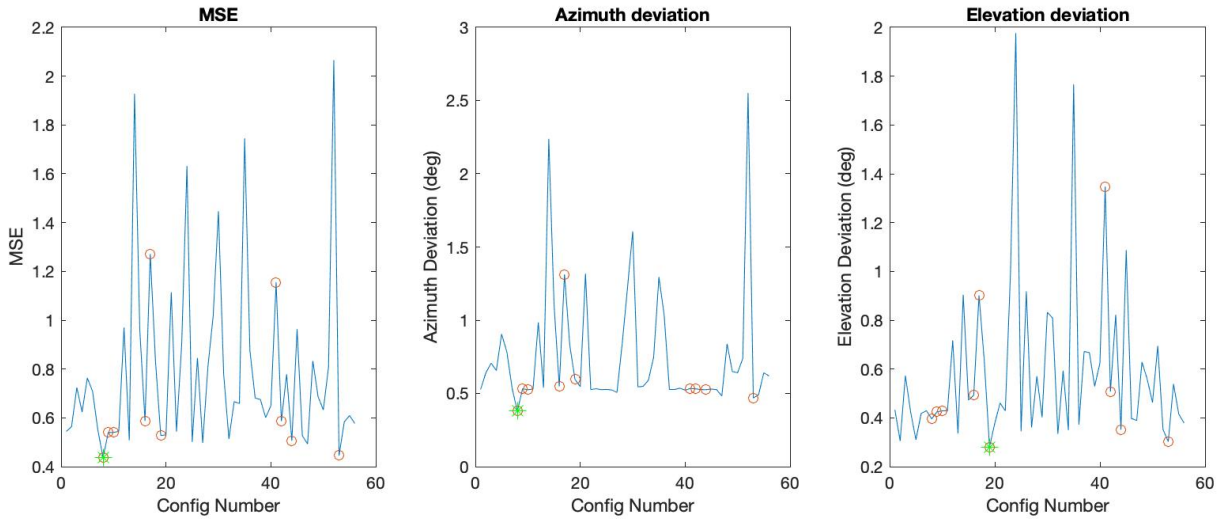


Figure 5.5: Errors obtained for all configurations when estimating position $s_{cart}(10,10,10)$

azimuth and the elevation deviations. In this case, this corresponds to configuration number 53 which reaches a mean deviation of 0.385 degrees.

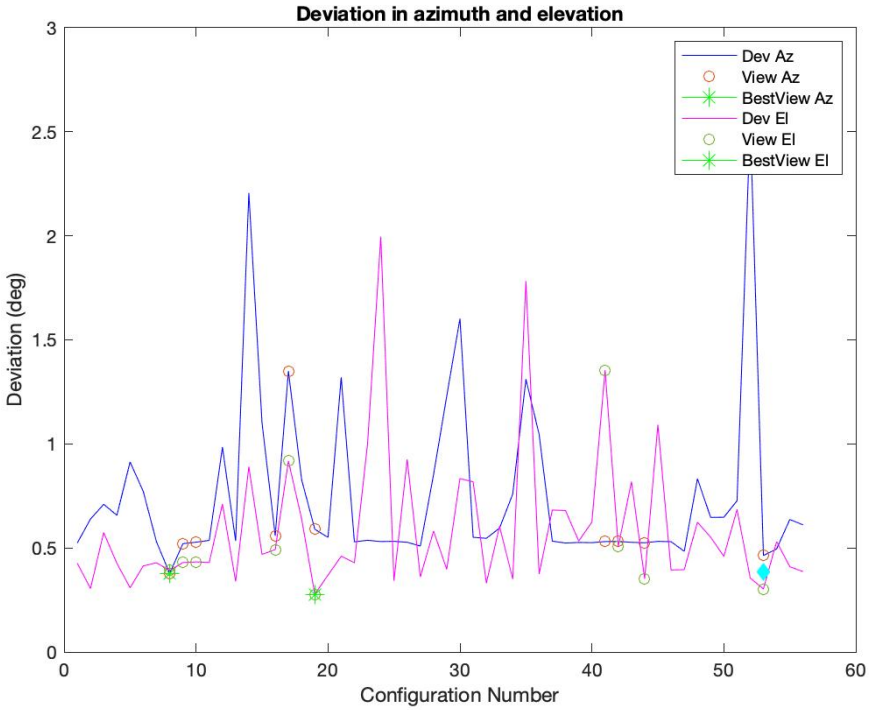


Figure 5.6: Overlaid azimuth and elevation deviations for all configurations when estimating position $s_{cart}(10,10,10)$

In a second experiment, position $s_{cart}(100,100,100)$ is tested, which has the same azimuth and

elevation angles as the previous position and a norm 10 times larger. For this case, the error range of azimuth and elevation estimation is approximately the same and the norm estimation presents an error around 10 times larger. Additionally, as expected the configurations that lead to the lowest errors are the same as for the first experiment.

A set of tests were executed in order to compare the performance of various positions estimation and to extract behavior patterns for the chosen configurations. The collected data is present in table 5.2, where the position of the transmitter are given in Cartesian coordinates by ($s_x$, $s_y$, $s_z$) and for each of the performance parameters it is presented the obtained best configuration number and the minimum error achieved by it. It should also be noted that the notation $0_+$/ $0_-$ indicates that for a theoretical position with a coordinate equal to zero it was returned a slightly positive/negative estimate of that same coordinate, due to the injected error.

| $s_{cart}$ | | | **Azimuth** | | **Elevation** | | **Azimuth+Elevation** | | **MSE** | |
|---|---|---|---|---|---|---|---|---|---|---|
| $x$ | $y$ | $z$ | Config | Min | Config | Min | Config | Min | Config | Min |
| 10 | 10 | 10 | 8 | 0.377 | 19 | 0.278 | 53 | 0.385 | 8 | 0.434 |
| -10 | -10 | -10 | 30 | 2.412 | 30 | 1.196 | 30 | 1.804 | 30 | 2.142 |
| $0_+$ | -10 | -10 | 14 | 2.058 | 14 | 0.431 | 14 | 1.244 | 14 | 1.672 |
| 100 | $0_-$ | $0_-$ | 47 | 0.177 | 32 | 0.177 | 11 | 0.284 | 11 | 0.330 |
| $0_+$ | 100 | $0_+$ | 9 | 0.596 | 16 | 0.425 | 16 | 0.512 | 16 | 0.586 |
| $0_+$ | $0_-$ | 100 | 37 | 52.572 | 39 | 0.381 | 37 | 26.479 | 39 | 32.602 |
| 15 | -10 | 5 | 48 | 0.364 | 3 | 0.218 | 27 | 0.346 | 27 | 0.399 |

Table 5.2: Summary of best configurations obtained by Monte Carlo simulation

Some conclusions can be taken upon the analysis of these results:

- Configurations that achieve the overall minimum errors tend to integrate the LOS hydrophones that attain the larger baseline between them;
- Transmitter positions that return a higher number of LOS hydrophones, have more possible configurations to choose from and therefore can be more optimized, presenting the lowest errors;
- The points directly behind the AUV that cover positions with $y$ and $z$ in the range [-w,w], are not contained in any line of sight region;
- When the transmitter positions have $x \leq 0$, they are in line of sight of less hydrophones than for $x > 0$, so there are fewer possible configurations and the returned best option for the various parameters are more consistent. Consequently, the returned minimum errors are usually higher than for $x > 0$;

- Transmitter positions that are located near the y-axis, almost in parallel with the circle of hydrophones, are usually covered by only four LOS regions, which correspond to the sensors that are directly closer to the target;

- For elevation angles close to $90^\circ$ and $-90^\circ$, the azimuth deviation is much larger than at any other position as expected, since in that region the azimuth angle is more influenced by the injected errors leading to increased deviations.

#### 5.2.0.1 Evaluation of the line of sight regions

Upon inspecting the overall obtained results and the whole function of the system, a particular analysis is conducted to the mechanism that defines the hydrophones' LOS regions. Therefore, after evaluating the position $s(10,10,10)$ that is expected to have an intermediate amount of hydrophones, two additional positions are tested.

The first position to be tested is $s(-10,-10,-10)$ which inherently has less hydrophones with line of sight, due to the method's limitation for $x \leq 0$. Additionally, since it is located in the seventh octant it is expected to be only in LOS with exactly three hydrophones, thus having only one available configuration with line of sight. After simulating, figure 5.7 is obtained which verifies the concepts described. The only configuration with line of sight is number 30, composed by $r_1$, $r_3$, $r_5$ and $r_9$.

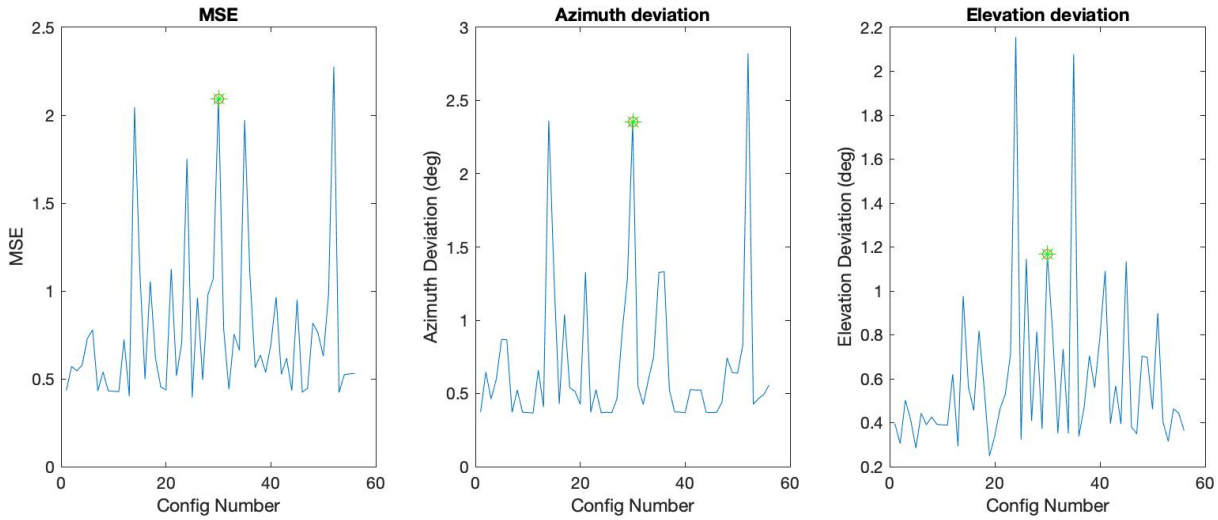


Figure 5.7: Errors obtained for all configurations when estimating position $s_{cart}(-10,-10,-10)$

Then, position $s(100,0,0)$ is tested. Due to its long range location and the fact that it is assumed a conic shape at the front of the vehicle, it is expected that this point has line of sight for every employed hydrophone. Figure 5.8 illustrates the simulated results which prove the theoretical expectation.

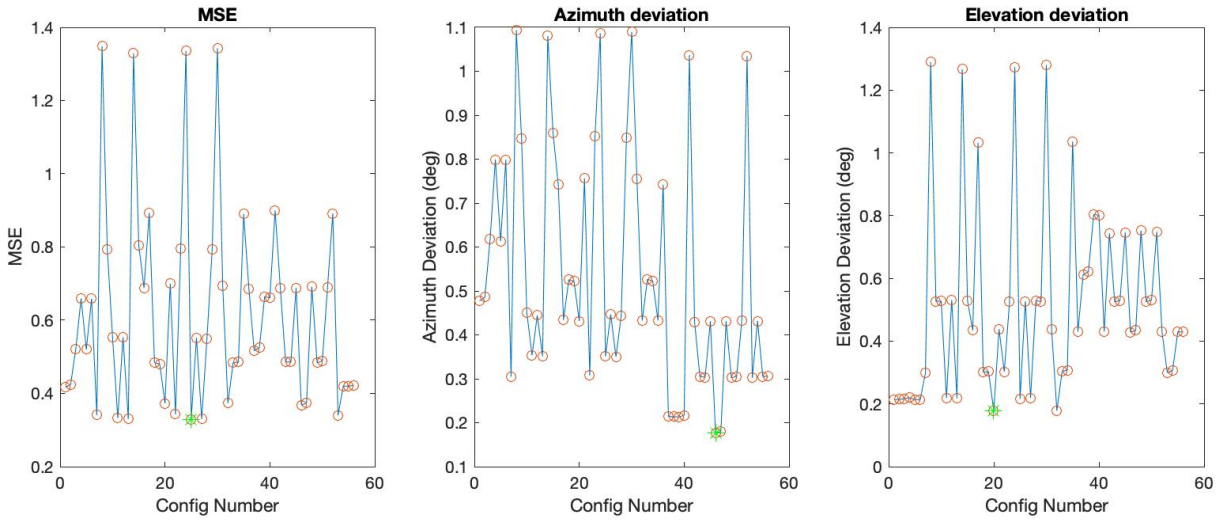


Figure 5.8: Errors obtained for all configurations when estimating position (100,0,0)

Lastly, an extensive verification process was held in order to ensure that the returned LOS hydrophones were plausible for many other positions. Table 5.3 summarizes this search, containing a total of eleven positions spread over each octant and the reference axis. By consulting the hydrophone map illustrated in 5.1, it is possible to confirm that for every selected position the returned hydrophones are the logically expected.

| | $s_x$ | $s_y$ | $s_z$ | Hydrophones with LOS |
|---|---|---|---|---|
| x-axis | 100 | 0 | 0 | 2, 3, 4, 5, 6, 7, 8, 9 |
| y-axis | 0 | 100 | 0 | 4, 6, 7 |
| z-axis | 0 | 0 | 100 | 2, 6, 8 |
| $1^{st}$ octant | 10 | 10 | 10 | 2, 4, 6, 7, 8 |
| $2^{nd}$ octant | 5 | 5 | -1 | 2, 3, 4, 6, 7 |
| $3^{rd}$ octant | 1 | -1 | 0 | 2, 3, 5, 8, 9 |
| $4^{th}$ octant | 1 | -10 | -10 | 3, 5, 7, 8, 9 |
| $5^{th}$ octant | -100 | 10 | 10 | 2, 4, 6 |
| $6^{th}$ octant | -1 | 10 | -5 | 3, 4, 6, 7 |
| $7^{th}$ octant | -1 | -1 | 1 | 2, 5, 8 |
| $8^{th}$ octant | -1 | -100 | -10 | 3, 5, 8, 9 |

Table 5.3: Hydrophones with line of sight for several $s$ positions

### 5.2.1 Comparison with Crámer-Rao lower bound

Although the Monte Carlo approach and the Crámer-Rao bound method use distinct decision metrics, it is still worth to understand the practical differences between the implementations regarding the developed dynamic reconfigurable method.

A simulation was performed in which position $s_{cart}(0, 1000, 0)$ is estimated by both methods, obtaining the estimate cloud by the Monte Carlo approach and the uncertainty axis in Crámer-Rao bound. Figure 5.9 illustrates both data overlaid, using configuration C.

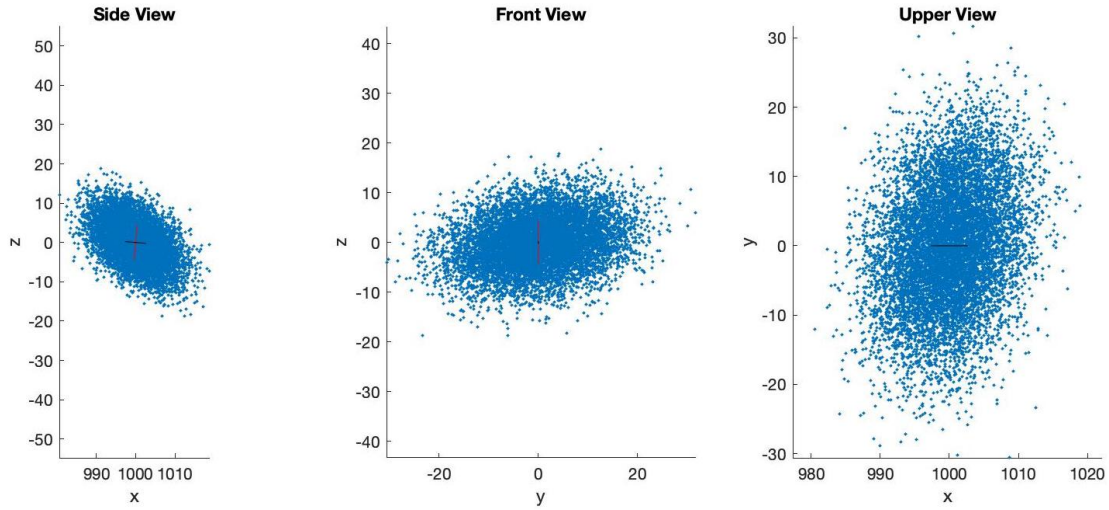


Figure 5.9: Errors obtained for all configurations when estimating position (100,0,0)

The plot reveals that the results are clearly not coherent, which is justified by the fact that the Crámer-Rao bound assumes any linear and unbiased estimator for the configuration's evaluation, while the Monte Carlo method is a non-linear estimator, due to the least squares equation that leads to the estimation in 4.2.2.

Therefore, to avoid lack of generalization, once more it is considered that the prefer mechanism to be used for analyzing the estimation accuracy is the FIM along with the desired optimality criteria.

## 5.3 Optimal solution based on range

After having a comprehensive understanding on the system that is capable of determining which is the best configuration of hydrophones to estimate a specific transmitter position, an alternate scenario can be explored. We now consider that the USBL system does not reconfigure which sensor configuration it should use in order to optimize the estimation in real time. Instead, a performance study is conducted beforehand so that only two configurations are chosen to be deployed, corresponding to the ones which return the average best estimation of short and long range positions. This way, it would be possible to alternate which configuration is used

depending solely on the distance to the target. Alternatively, it is also possible to define just one overall best configuration, in cases where there is the necessity of reducing the number of deployed hydrophones or if the two obtained configurations do not have a significant difference in performance.

In the development of this mechanism, there are some adjustments and similarities from the conditions established for the previous system. Firstly, it is assumed that the hydrophones are implemented in a structure shaped like an AUV with no physical form, thus all hydrophone positions have line of sight to any point in space. Additionally, the possibilities for the hydrophone locations are increased for a more extensive study. Once again, hydrophone $r_1$ is integrated in all configurations and a total of 24 possibilities are considered for the remnant three. These include the same 8 positions $r_2$ to $r_9$, established for the initial setup, to which are added positions $r_{10}$ to $r_{25}$ defined in table 5.4. This addition corresponds to two replicated circles from the initial one, that assume the same $y$ and $z$ coordinates but are deviated from each other a $d\_x$ equal to 20 centimeters. Figure 5.10 illustrates all the considered possible positions for the hydrophone's deployment. Accordingly, the number of possibilities is not correspondent to combinations of three out of 24, $C(24,3)$, since these contain linearly dependent configurations, which correspond to hydrophones' positions that only differ in the $x$ coordinate. Therefore, the total number of available combinations is 1512.

| | $r_{10}$ | $r_{11}$ | $r_{12}$ | $r_{13}$ | $r_{14}$ | $r_{15}$ | $r_{16}$ | $r_{17}$ | $r_{18}$ | $r_{19}$ | $r_{20}$ | $r_{21}$ | $r_{22}$ | $r_{23}$ | $r_{24}$ | $r_{25}$ |
|---|---|---|---|---|---|---|---|---|---|---|---|---|---|---|---|---|
| x | 0 | 0 | 0 | 0 | 0 | 0 | 0 | 0 | $d\_x$ | $d\_x$ | $d\_x$ | $d\_x$ | $d\_x$ | $d\_x$ | $d\_x$ | $d\_x$ |
| y | 0 | 0 | w | -w | e | e | -e | -e | 0 | 0 | w | -w | e | e | -e | -e |
| z | w | -w | 0 | 0 | e | -e | e | -e | w | -w | 0 | 0 | e | -e | e | -e |

Table 5.4: Additional coordinates for an implementation with 25 hydrophones

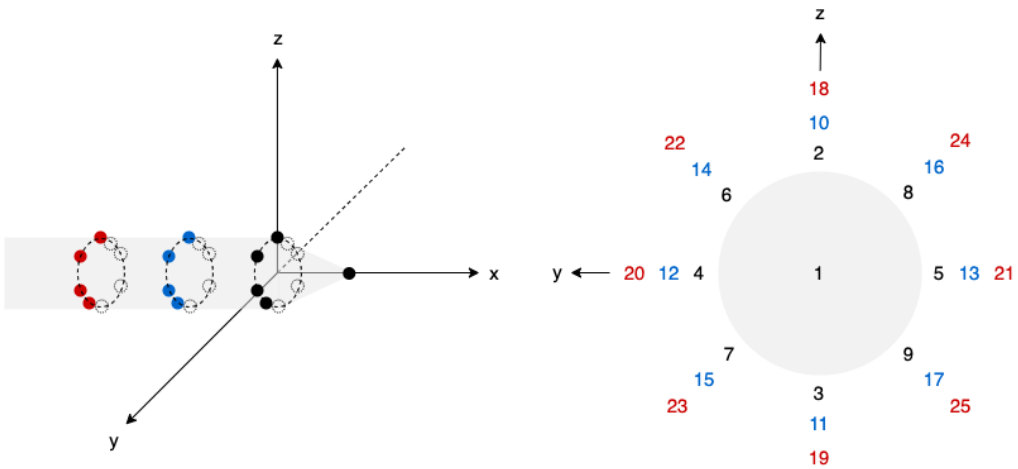


Figure 5.10: Hydrophone possible positions for optimality study based on range

The applied algorithm is similar to the previously explained algorithms 1 and 2, with the following variations:

1. Similarly to the condition described in 4.2.5, the acoustic source positions, $s$, to be estimated are defined in spherical coordinates, where for each defined norm, the elevation component covers the interval [-90° to 90°] in steps of one and, for each elevation value, the azimuth component covers the interval [-180°, 180°] in steps of one, forming partial spheres around the reference axis' origin. The norm covers a range between 1 and 10000 meters.

2. An additional logical loop is added in algorithm 1 between lines 1 and 2, so that for each possible configuration all $s$ are estimated a number of $i = 1000$ iterations.

3. the $line\_of\_sight$ function is no longer used, as it is considered that all hydrophones have line of sight to every position $s$.

From here it is possible to analyze which are the best returned configurations, according to the chosen parameters MSE, azimuth deviation, elevation deviation and combined azimuth and elevation deviations. According to the numeric errors that are obtained, it is then possible to decide whether there is a single configuration that has evidently a better performance than the others or if there is a pair of configurations that can be used to obtain individually better estimations for short and long range.

### 5.3.1 Simulation results

The previously defined method was tested through a series of simulations, in which all 1512 defined configurations repeatedly estimate all positions that compose spheres of defined norms. Then, the configurations that reveals lower estimation errors are selected as the most accurate in terms of azimuth angle, elevation angle, both angles simultaneously or MSE.

The overall results do not demonstrate a specific configuration to be the clear best in short or long range for the chosen parameters. In order to associate the obtained configuration numbers to the actual hydrophone placement, figure 5.11 gathers the most relevant representations for the simulations based on range.

For performance based on azimuth, configuration number 792 shows best results for norms between 1 and 10 meters. However, for longer range the results do not tends to a specific configuration, alternating between three options.

Regarding performance based on elevation, configuration 220 is indicated for 1 to 3 meters, while for ranges going from 10 to 10000 meters, configuration 260 is the clear preferred. As can be observed in the illustration, these are structurally similar.

When evaluating azimuth and elevation accuracy simultaneously or MSE, the results are not clear and many configurations are alternated, where number 827 is the most frequent.

Additionally, it should be noted that throughout all simulated norms, for each evaluated metrics the worse performance for every position corresponded to the same configurations.

| | **Azimuth** | | **Elevation** | | **Azimuth+Elevation** | | **MSE** | |
|---|---|---|---|---|---|---|---|---|
| Norm | Config | Min | Config | Min | Config | Min | Config | Min |
| 1 | 792 | 0.4730 | 220 | 0.1758 | 862 | 0.3554 | 862 | 0.4654 |
| 2 | 792 | 0.4771 | 220 | 0.1738 | 827 | 0.3905 | 827 | 0.4549 |
| 3 | 792 | 0.4820 | 220 | 0.1752 | 827 | 0.3921 | 860 | 0.4571 |
| 10 | 792 | 0.4796 | 260 | 0.1702 | 827 | 0.3918 | 827 | 0.4572 |
| 20 | 827 | 0.4893 | 260 | 0.1702 | 827 | 0.3905 | 827 | 0.4537 |
| 50 | 792 | 0.4940 | 220 | 0.1705 | 860 | 0.3947 | 860 | 0.4615 |
| 100 | 860 | 0.4881 | 260 | 0.1707 | 827 | 0.3913 | 860 | 0.4538 |
| 200 | 827 | 0.4853 | 260 | 0.1706 | 827 | 0.3889 | 827 | 0.4511 |
| 500 | 792 | 0.4886 | 260 | 0.1722 | 929 | 0.3935 | 862 | 0.4606 |
| 1000 | 827 | 0.4846 | 260 | 0.1709 | 827 | 0.3899 | 827 | 0.4524 |
| 10000 | 792 | 0.4810 | 260 | 0.1724 | 862 | 0.3920 | 827 | 0.4554 |

Table 5.5: Results of Monte Carlo simulation for range based estimation

To conclude, the obtained data do not show a clear tendency of two specific configurations being overall best for short and long range. This can be a result of the Monte Carlo simulation nature which originates results that do not have a clear sequence as expected. Therefore, this same experiment is repeated in the next subsection using the Fisher Information Matrix integrated in the Crámer-Rao bound method.

### 5.3.2 FIM simulation

Since the Fisher Information Matrix is a reliable and well know tool for evaluating a configuration's performance, then a simulation was executed for determining the best configuration for short and long range estimations. Therefore, the method was integrated in a Monte Carlo approach that tests all 1512 configurations defined previously described in this section, which integrate a total of 25 different hydrophones. For each configuration, all $s$ positions that make up a sphere with a defined norm are used to calculate the FIM and evaluate the desired criteria. Among all, the configurations that demonstrate the preferred results correspond to the best performance in each specific criteria.

Table 5.6 summarizes the obtained results for a norm range between 1 and 10000 meters. A standard metric and three optimality criteria were observed and for each of them, the table indicates the configuration number that proved to have the best performance and the respective achieved values:

- In E-optimality, the Eigenvalue column contains the minimum larger eigenvalue found among all configurations

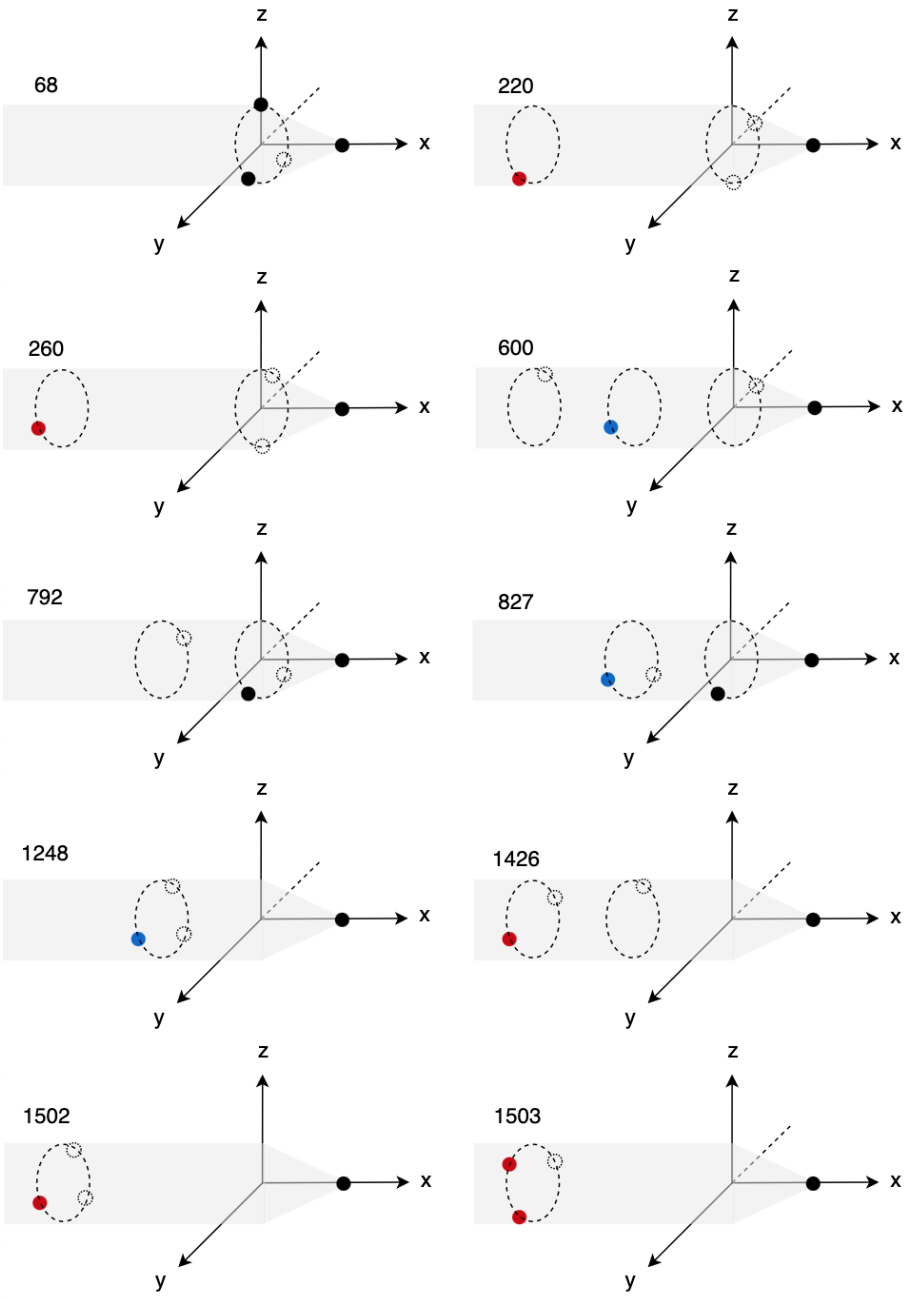


Figure 5.11: Illustration of relevant hydrophone configurations for range based estimation

- In D-optimality, the Determinant column includes the minimum computed determinant of the inverse of the FIM for all configurations
- In A-optimality, the Trace column comprises the minimum sum of eigenvalues of the FIM among all configurations

The overall results do not demonstrate a specific configuration to be the clear best in short or long range for the chosen parameters. In order to associate the obtained configuration numbers

| | **E-optimality** | | **D-Optimality** | | **A-Optimality** | |
|---|---|---|---|---|---|---|
| Norm | Config | Eigenvalue | Config | Determinant | Config | Trace |
| 1 | 1248 | $6.2\times10^{-3}$ | 1503 | $1.6\times10^{-3}$ | 600 | $2.3\times10^{-5}$ |
| 2 | 1248 | 0.012 | 1503 | $2.5\times10^{-3}$ | 1426 | $9.2\times10^{-5}$ |
| 3 | 1248 | 0.018 | 1503 | $3.3\times10^{-3}$ | 1426 | $2.1\times10^{-4}$ |
| 10 | 1502 | 0.061 | 1503 | $7.4\times10^{-3}$ | 1426 | $2.4\times10^{-3}$ |
| 20 | 1502 | 0.121 | 1503 | 0.012 | 1426 | $9.6\times10^{-3}$ |
| 50 | 1502 | 0.303 | 1503 | 0.022 | 1426 | 0.061 |
| 100 | 1502 | 0.061 | 1503 | 0.034 | 1426 | 0.242 |
| 200 | 1502 | 1.212 | 1503 | 0.054 | 1426 | 0.968 |
| 500 | 1502 | 3.029 | 1503 | 0.100 | 1426 | 6.055 |
| 1000 | 1502 | 6.059 | 1503 | 0.159 | 1426 | 24.226 |
| 10000 | 1502 | 60.587 | 1503 | 0.737 | 1426 | $2.42\times10^{3}$ |

Table 5.6: Results of FIM simulation for range based estimation

to the actual hydrophone placement, figure 5.11 gathers the most relevant representations for the simulations based on range.

By inspection, it is possible to understand that for each criterion there is a clear best configuration for short and long range. The hydrophone placement of the mentioned configuration numbers are illustrated in figure 5.11 for a more practical interpretation.

Therefore, in terms of E-optimality configuration, an approximately constant error of 0.6% is visible, where number 1248 shows the best performance for range between 1 and 3 meters, while from 10 to 10000 meters configuration 1502 is considered the best.

For D-optimality, a single configuration, number 1503, was considered the best for all defined ranges, which corresponds to an hydrophone placement that maximizes the baseline between the fixed sensor and the other three.

Finally, in terms of A-optimality configuration number 600 is indicated for norm equal to 1 meters and, for the remaining ranges, number 1426 is chosen as the preferable option.

## 5.4 Summary and Discussion

This chapter focuses on presenting the formulated adaptive configuration selection method, whose goal is to establish the sensor configuration that leads to the best estimation precision for a specific target position. After analyzing the results, it has proven to provide improved estimation accuracy by selecting the configuration with line of sight to the target that achieves the lower estimation error.

This mechanism could be applied to a data muling scenario, as established in chapter 1. If a discrete set of hydrophones are deployed in an mule AUV, then it is possible to adapt the selected configuration depending on the perceived angle of arrival in real-time. This allows to always use the configuration that leads to the lower estimation error and thus improve the localization accuracy.

An alternative to this method is also explored, whose goal is to select the sensor configuration that achieves the average best estimation for any target position along a sphere of defined norm. This allows to define optimal configurations based on the range, as demonstrated through simulations. As observed previously, the results of the Crámer-Rao lower bound demonstrate clear optimal configurations for both short and long range.

In practical terms, this would be useful if a maximum of two possible configurations were allowed to be deployed in an AUV, contrarily to the initial method. Considering the E-optimality as the most relevant criterion for this application, we can conclude that for short range configuration number 1248 would be optimal, whereas for long range number 1502 would be preferred.

# Chapter 6

# Conclusions

## 6.1 Summary

As stated at the beginning, the overall aim of this research work was to develop a USBL system with characteristics that lead to an improvement on localization precision, both for short and long range.

Firstly, it is presented the implementation of an hardware module that computes with precision the time differences of arrival of acoustic signals received by a set of four hydrophones. The architecture demonstrated a significant decrease of the used resources comparatively to the previous implementation and a precise calculation of the time differences of arrival. After initial field tests, a rough estimation of the obtained precision leads to conclude that the ToA measurement was improved by using the phase differences along with the correlation.

Secondly, an adaptive configuration selection method was developed which is capable of determining the optimal configuration from a discrete set of fixed hydrophones, leading to higher localization precision, i.e. lower estimation error. It uses a Monte Carlo approach for a systematic comparison between a high number of configurations and to obtain averaged estimations for more coherent results. Additionally, as an effort to improve the USBL system's viewing angle, it was integrated a mechanism that assures the continuous selection of hydrophone sets that have line of sight to the transmitter positions. The simulated results show that the method as proven to be successful, since the selected configurations always correspond to the layout that leads to the lower estimation error.

Additionally, as initially intended, the method was adjusted so that it was possible to conduct a comprehensive study on the configurations that demonstrated to be optimal for short and long range. It was concluded that using the FIM together with the preferred optimality criterion for this application, originated the most coherent results and allowed to elect the configurations that lead to an average higher precision.

This evaluation tool can be applied to any method that is capable of defining performance metrics for the evaluation of a sensor configuration. In the present research work three options were investigated, consisting on an estimator based on the TDoA measurement, an estimator that

assumes a plane wavefront and the Crámer-Rao lower bound that uses the Fisher Information Matrix. From these three options, it was concluded that the most reliable would be the third due to the independence on the chosen estimator and its wide use on literature.

## 6.2 Contributions

The main contributions of this dissertation are:

- A HDL system design with strict area constraints that receives signals from four different sensors and calculates the phase differences between them;
- A comparative study on three methods that evaluate the performance of sensor configurations based on several different optimality criteria;
- The adaptive configuration selection method which is capable of determining the optimal sensor configuration, from a discrete set of hydrophones in fixed positions, that leads to highest localization precision, i.e. lowest estimation error.

## 6.3 Future Work

The developed work arose various innovative ideas and topics according to the state of the art on localization optimization methods. Therefore, there is the intent to produce a a scientific article on the subject to be submitted in the OCEANS Conference 2021.

The adopted optimization techniques in the present work are the starting point of a topic which is not very explored in the current literature. Consequently, there are several areas that can be improved as follows:

- Implementing the developed algorithm for AoA estimation as a real-time system which can be used for decision making during underwater navigation;
- Using Machine Learning techniques in order to find the optimal hydrophone array configuration, to be positioned in an underwater vehicle;
- Integrating the estimator with a Kalman Filter or a Particle Swarm Optimization approach;
- Perform field experiments in order to examine if it is advantageous to select only the hydrophones with line of sight or if the errors obtained from propagation in the surface of the AUV are negligible;

# Appendix A

# Complementary Information

## A.1 Hydrophone configurations numeration

In table A.1 it is possible to consult the composition of the configurations which are mentioned throughout the document. It includes the configuration number and the respective integrated hydrophones.

Table A.1: Configurations for the Monte Carlo approach with 9 employed hydrophones

| Configuration number | Hydrophones |
|---|---|
| 1 | 1 2 3 4 |
| 2 | 1 2 3 5 |
| 3 | 1 2 3 6 |
| 4 | 1 2 3 7 |
| 5 | 1 2 3 8 |
| 6 | 1 2 3 9 |
| 7 | 1 2 4 5 |
| 8 | 1 2 4 6 |
| 9 | 1 2 4 7 |
| 10 | 1 2 4 8 |
| 11 | 1 2 4 9 |
| 12 | 1 2 5 6 |
| 13 | 1 2 5 7 |
| 14 | 1 2 5 8 |
| 15 | 1 2 5 9 |

**Table A.1**

| Configuration number | Hydrophones | | | |
|---|---|---|---|---|
| 16 | 1 | 2 | 6 | 7 |
| 17 | 1 | 2 | 6 | 8 |
| 18 | 1 | 2 | 6 | 9 |
| 19 | 1 | 2 | 7 | 8 |
| 20 | 1 | 2 | 7 | 9 |
| 21 | 1 | 2 | 8 | 9 |
| 22 | 1 | 3 | 4 | 5 |
| 23 | 1 | 3 | 4 | 6 |
| 24 | 1 | 3 | 4 | 7 |
| 25 | 1 | 3 | 4 | 8 |
| 26 | 1 | 3 | 4 | 9 |
| 27 | 1 | 3 | 5 | 6 |
| 28 | 1 | 3 | 5 | 7 |
| 29 | 1 | 3 | 5 | 8 |
| 30 | 1 | 3 | 5 | 9 |
| 31 | 1 | 3 | 6 | 7 |
| 32 | 1 | 3 | 6 | 8 |
| 33 | 1 | 3 | 6 | 9 |
| 34 | 1 | 3 | 7 | 8 |
| 35 | 1 | 3 | 7 | 9 |
| 36 | 1 | 3 | 8 | 9 |
| 37 | 1 | 4 | 5 | 6 |
| 38 | 1 | 4 | 5 | 7 |
| 39 | 1 | 4 | 5 | 8 |
| 40 | 1 | 4 | 5 | 9 |
| 41 | 1 | 4 | 6 | 7 |
| 42 | 1 | 4 | 6 | 8 |
| 43 | 1 | 4 | 6 | 9 |

**Table A.1**

| Configuration number | Hydrophones |
|---|---|
| 44 | 1 4 7 8 |
| 45 | 1 4 7 9 |
| 46 | 1 4 8 9 |
| 47 | 1 5 6 7 |
| 48 | 1 5 6 8 |
| 49 | 1 5 6 9 |
| 50 | 1 5 7 8 |
| 51 | 1 5 7 9 |
| 52 | 1 5 8 9 |
| 53 | 1 6 7 8 |
| 54 | 1 6 7 9 |
| 55 | 1 6 8 9 |
| 56 | 1 7 8 9 |

# References


[1] J. Liang, "Fifteen percent of ocean floor now mapped," Jun 2019. [Online] Available: https://www.deeperblue.com/fifteen-percent-of-ocean-floor-now-mapped/. [Accessed Oct. 28, 2019].

[2] H. P. Tan, R. Diamant, W. K. G. Seah, and M. Waldmeyer, "A survey of techniques and challenges in underwater localization," *Ocean Engineering*, vol. 38, no. 1, pp. 1663–1676, 2011.

[3] F. B. Jensen, W. A. Kuperman, M. B. Porter, and H. Schmidt, "Fundamentals of Ocean Acoustics," in *Computational Ocean Acoustics*, pp. 3–17, Springer Science & Business Media, second ed., 2011.

[4] M. C. Domingo, "Overview of channel models for underwater wireless communication networks," *Physical Communication*, vol. 1, no. 3, pp. 163–182, 2008.

[5] M. Stojanovic and J. Preisig, "Underwater Acoustic Communication Channels: Propagation Models and Statistical Characterization," *IEEE Communications Magazine*, vol. 47, no. 1, pp. 84–89, 2009.

[6] J. M. F. M. aes, "Improving Time of Arrival Estimation Using Encoded Acoustic Signals," Master's thesis, Faculty of Engineering of the University of Porto, Porto, jul 2018.

[7] D. E. Chaitanya, C. V. Sridevi, and G. S. B. Rao, "Path loss analysis of Underwater communication systems," in *IEEE Technology Students' Symposium*, pp. 65–70, IEEE, 2011.

[8] S. Gezici, "A survey on wireless position estimation," *Wireless Personal Communications*, vol. 44, no. 3, p. 263–282, 2008. Springer Science & Business Media.

[9] B. M. R. Bharathi and A. R. Mohanty, "Underwater Sound Source Localization by EMD-Based Maximum Likelihood Method," *Acoustics Australia*, vol. 46, no. 2, pp. 193–203, 2018.

[10] V. Chandrasekhar, W. K. Seah, Y. S. Choo, and H. V. Ee, "Localization in underwater sensor networks: survey and challenges," in *WUWNet '06: Proceedings of the 1st ACM international workshop on Underwater networks*, pp. 33–40, 2006.

[11] J. Esteves, A. Carvalho, and C. Couto, "Generalized geometric triangulation algorithm for mobile robot absolute self-localization," in *2003 IEEE International Symposium on Industrial Electronics*, vol. 1, (Rio de Janeiro, Brazil), pp. 346–351, 2003.

[12] A. P. Pandian, T. Senjyu, S. M. S. Islam, and H. Wang, "Weighted Trilateratiton and Centroid Combined Indoor Localization in Wifi Based Sensor Network," in *Proceeding of the International Conference on Computer Networks, Big Data and IoT (ICCBI - 2018)*, pp. 163–166, jul 2019.

[13] M. Erol-Kantarci, H. T. Mouftah, and S. Oktug, "A Survey of Architectures and Localization Techniques for Underwater Acoustic Sensor Networks," *IEEE Communications Surveys & Tutorials*, vol. 13, no. 3, pp. 487–502, 2011.

[14] X. You, Y. Wu, M. Zhu, X. Li, and L. Zhang, "Low Complexity Short Baseline Localization Algorithm Based on Taylor Expansion," in *2019 IEEE International Conference on Signal Processing, Communications and Computing*, pp. 1–5, IEEE, 2019.

[15] K. G. Kebkala and A. I. Mashoshinc., "AUV Acoustic Positioning Methods," *Gyroscopy and Navigation*, vol. 8, pp. 80–89, sep 2017.

[16] D. Sun, J. Ding, C. Zheng, and W. Huang, "An Underwater Acoustic Positioning Algorithm for Compact Arrays With Arbitrary Configuration," *IEEE Journal of Selected Topics in Signal Processing*, vol. 13, pp. 120–130, mar 2019.

[17] E. GmbH, "Underwater USBL Positioning Systems," 2018. [Online] Available: https://evologics.de/usbl. [Accessed Jan. 26, 2020].

[18] E. GmbH, "S2C Technology," 2018. [Online]. Available: https://evologics.de/s2c-technology [Accessed Jan. 26, 2020].

[19] E. GmbH, "18/34 communication and positioning devices," 2018. [Online]. Available: https://evologics.de/acoustic-modem/18-34 [Accessed Jan. 26, 2020].

[20] E. GmbH, "S2C R 12/24 USBL communication and positioning device," 2018. [Online]. Available: https://evologics.de/acoustic-modem/12-24/usbl-serie [Accessed Jan. 26, 2020].

[21] Sonardyne, "MICRO-RANGER 2 SHALLOW WATER USBL SYSTEM," 2020. [Online]. Available: https://www.sonardyne.com/product/micro-ranger-2-shallow-water-usbl-system/ [Accessed Feb. 3, 2020].

[22] K. Maritime, "HiPAP - HIGH PRECISION ACOUSTIC POSITIONING," 2016. [Online]. Available: https://www.kongsberg.com/maritime/products/Acoustics-Positioning-and-Communication/acoustic-positioning-systems/hipap-models/ [Accessed May 2, 2020].

[23] A. N. Bishop, B. Fidan, B. D. O. Anderson, K. Doğançay, and P. N. Pathirana, "Optimality analysis of sensor-target localization geometries," *Automatica*, vol. 46, no. 3, pp. 479–492, 2010.

[24] E. Rady, M. M. E. A. El-Monsef, and M. M. Seyam, "Relationships among several optimality criteria," *Interstat*, vol. 15, no. 6, pp. 1–11, 2009.

[25] C. Tholen, T. A. El-Mihoub, L. Nolle, O. Ralle, and R. Rofallski, "Optimal receiver configuration of short-baseline localisation systems using particle swarm optimisation.," in *ECMS*, pp. 25–31, 2020.

[26] A. M. Bonito, "Acoustic system for ground truth underwater positioning in DEEC's test tank," Master's thesis, Faculty of Engineering of the University of Porto, Porto, jul 2019.

[27] J. Valls, T. Sansaloni, A. Perez-Pascual, V. Torres, and V. Almenar, "The use of cordic in software defined radios: A tutorial," *IEEE Communications Magazine*, vol. 44, no. 9, pp. 46–50, 2006.

[28] A. A. Assef, B. M. Ferreira, J. M. Maia, and E. T. Costa, "Modeling and fpga-based implementation of an efficient and simple envelope detector using a hilbert transform fir filter for ultrasound imaging applications," *Research on Biomedical Engineering*, vol. 34, no. 1, pp. 87–92, 2018.

[29] J. Reis, M. Morgado, P. Batista, P. Oliveira, and C. Silvestre, "Design and experimental validation of a usbl underwater acoustic positioning system," *Sensors*, vol. 16, no. 9, p. 1491, 2016.

[30] B. Ferreira, A. Matos, and N. Cruz, "Optimal positioning of autonomous marine vehicles for underwater acoustic source localization using TOA measurements," in *2013 IEEE International Underwater Technology Symposium (UT)*, pp. 1–7, IEEE, 2013.